ESCUELA TÉCNICA SUPERIOR DE INGENIEROS INDUSTRIALES Y DE TELECOMUNICACIÓN

UNIVERSIDAD DE CANTABRIA

European Project Semester
Undergraduate Thesis

Performance simulation of Hydrogen streams in an internal combustion engine.

(Simulación del rendimiento de corrientes de hidrógeno en un motor de combustión interna.)

Para acceder al Título de

Graduado en Ingeniería Química

Author: Fabián Musy Palacio

June 2021

Acknowledgements

First of all, thanks to my tutors Alfredo Ortiz and Rafael Ortiz-Imedio for guiding me and helping me at all times, without them, the completion of this thesis would not have been possible. I am especially grateful to Rafael for all the time he spent transmitting his knowledge to me and for always being willing to resolve any doubts I encountered.

To my fellow students, who have lived with me during these four years, and some of whom I consider true friends.

To my mother, for being the most important person in my life, my role model and an example in every way, as well as my grandmother, for raising me, loving me and always taking care of me together with my cousins and my aunt, I wouldn't change you for anything, I love you.

To my father, for loving me as much as I love him, always encouraging me to achieve my goals and telling me that I can achieve whatever I set my mind to.

To those who are no longer here to celebrate with me, especially my grandfather César, for teaching me to treat people with respect, to be humble, honest and a good person, I miss you.

To my friends, in particular to Leo, for being the person who understands me best in the world, gives me the best advice and always knows how to get the best out of me, I love you like a brother.

Table of contents

List of Figures.

List of Tables.

1. Introduction.

1.1. Technological adaptation of different decarbonisation systems.

The European Green Deal has been implemented in the European Union (EU), incentivising further decarbonisation of the energy system that is required to meet 2030 and 2050 climate targets [1]. For this reason, a wide variety of mitigation technologies are being developed to contribute to energy system decarbonisation [2].

1.1.1. Decarbonisation of Industry: Power sector and manufacturing industry.

These goals cannot be achieved without energy savings in the manufacturing industry, which uses around 25 % of the total final energy use in Europe [3]. Therefore, a power sector mostly based on renewable sources such as solar, wind, hydraulic or hydroelectric, biomass, biogas, and geothermal should be boosted [1]. In that way, energy efficiency must be prioritised and improved in a cost-effective way [3]. For this reason, some manufacturers have been started to work with hydrogen (H_2), because of its wide range of applications as an energetic vector, such as refinery processes like hydrodesulfurization and hydrocracking, ammonia production, methanol production, in the food industry for vegetable oils hydrogenation, in bituminous to refine the synthetic crude into value-added products such as gasoline and diesel, as reducer reagent in the metallurgical industry, to produce flat glass, and producing synthetic fuels by hydrogenation. Finally, some important uses of H_2 can be seen in Figure 1.1 [4].

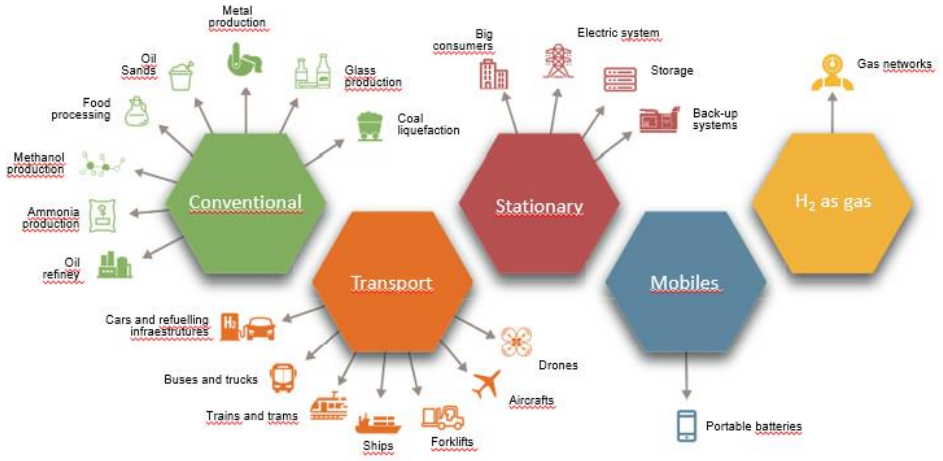

Figure 1.1 Uses of hydrogen as an energy vector [4].

1.1.2. Decarbonization of transport sector: New Fuels.

The introduction of alternative fuels drives the emergence of novel technologies some of them based on implementation or adaptation in mature technologies. This enables the use of new fuels, achieving a cost reduction while reducing emissions. Although new fuels like hydrogen (H_2) can be used in industrial applications, for instance, in gas turbines, the main goal remains in their use in the transport sector. In this sense, power-to-X applications have been recently promoted in Europe and have found the most promising market in green mobility, applying the power-to-fuel model, which is mostly based on the use of H_2, and synthetic methane (CH_4) as an interesting alternative to conventional fossil fuels [5].

1.2. The role of hydrogen in transport mobility.

The "hydrogen mobility" based on the hydrogen internal combustion engine (H_2-ICE) and the hydrogen Fuel Cells (FCs) are the two main pillars of this mobility solution [6]. In the case of H_2 FCs, they are based on the H_2 oxidation to produce electric energy for powering Fuel Cell Electric Vehicles (FCEVs), obtaining water vapour (H_2O (g)) as exhaust gases [7]. In addition, FCs can be classified according to the type of the membrane as Proton Exchange Membrane (PEMFCs), Alkaline, Phosphoric acid (PAFCs), Molten Carbonate (MOFCs) and Solid Oxide FCs (SOFCs), that are used in different applications depending on operating conditions such as temperature [7]**.** However, compared to the H_2-ICEs the FCEVs have some drawbacks, such as the costs of manufacturing, the issues in batteries disposal and their waste management and the scarcity together with the high costs associated with the materials to produce them such as Platinum (Pt) [6]. For this reason, the H_2-ICEs are the most suitable option today, and the production and proper use of H_2 based on its properties is a relevant issue.

1.2.1. Hydrogen production.

In terms of energy efficiency, cost savings and environmental sustainability, currently exist two main different ways to obtain H_2:

- Steam methane reforming (SMR):

This operation is based on the reforming reaction, from natural gas mainly composed of CH_4 and H_2O steam lead by a nickel (Ni) catalyst at high temperatures (800 ºC), enhancing the reaction between CH_4 and the H_2-O molecules from the steam, where syngas ($CO+H_2$) is produced (9). Then, the water gas shift reaction between the CO and steam over the Ni catalyst surface takes place, forming H_2 and CO_2 in two different stages, first at the High-Temperature Stage (HTS) and then at Low-Temperature Stage (LTS). Finally, to reduce the impacts from CO and CO_2, and removing the impurities of the H_2, the process requires further purification by applying CO_2 removal and methanation. In Figure 1.2 the process with the stoichiometric reactions has been depicted [8].

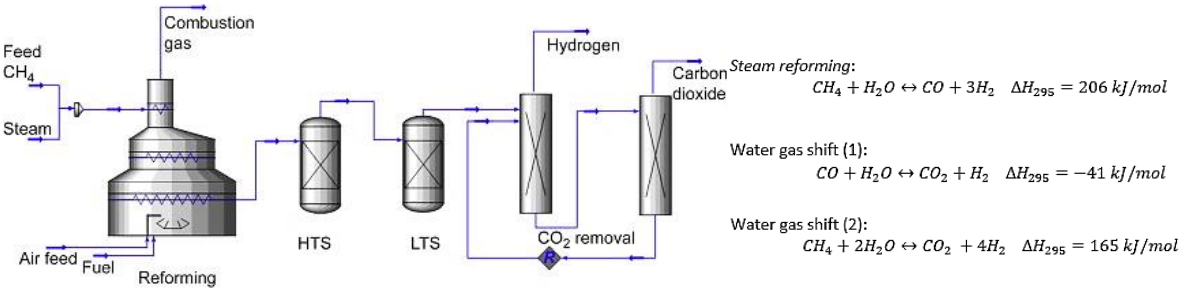

Figure 1.2. Steam Methane Reforming process to produce hydrogen [8].

- Electrolysis:

This is the most used technique for green hydrogen production, based on an electro separation method. The unit is arranged by cells, operating mostly in parallel at an industrial scale, so H_2O enters the cell and then is decomposed into H_2 and O_2, applying a direct current [7]. The cell is based on two separated electrodes, anode, and cathode, separated by an electrolyte layer [9]. Moreover, there are a lot of alternatives of the same process, for instance; alkaline electrolysers (ALK), proton exchange membrane electrolysers (PEM), anion exchange membrane (AEM) and solid oxide electrolyser (SOEC), showed in Figure 1.3 [9].

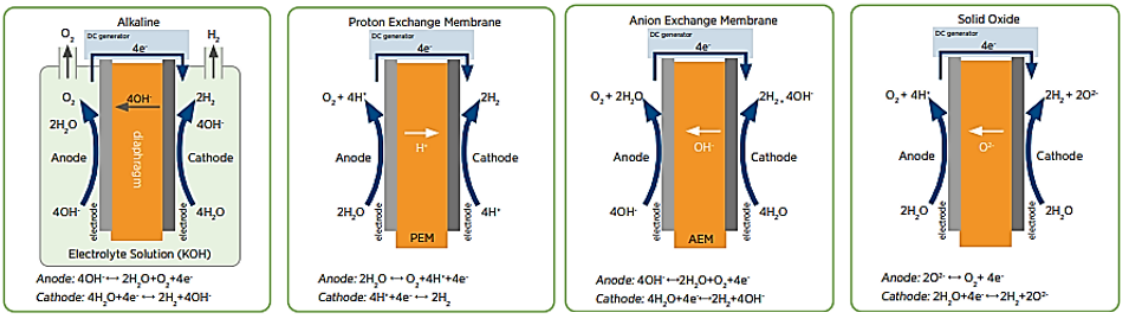

Figure 1.3. Different types of Electrolysis technologies [9].

1.2.2. Properties as fuel: Comparative study with fossil fuels.

The differences between fossil fuels and H_2, determine the operational conditions and performances in the Internal Combustion Engines (ICEs), due to the relation between their behaviour and the properties, as can be seen below in Table 1.1 [10].

Table 1.1. Physicochemical properties of fuels at 273.15 K and 10^5 Pa [10].

Parameter	Unit	Gasoline	Diesel	Hydrogen
Chemical Formula		C_4-C_{12}	C_8-C_{25}	H_2
Composition (C, H, O)	Mass-%	86, 14, 0	87, 13, 0	0, 100, 0
Lower heating value (LHV)	MJ/kg	42.7	42.78	120
Density	kg/m^3	720-780	848	0.089
Stoichiometric air/fuel ratio	kg/kg	14.7	14.5	34.3
Flammability limits	Vol-% ϕ	1.0-7.6 0.7-2.6	1.0-6 0.7-2.2	4-75 0.1-6
Laminar flame speed	m/s	0.35-0.50	N.A.	2.85-3.25
Auto-ignition temperature	ºC	≈ 350	≈ 265	585

From Table 1.1 can be extracted several conclusions. First, in an ICEs based on the higher "lower heating value" (LHV) and lower density of H_2, a bigger volume is filled which results in lower quantities of fresh air in the intake and lower volumetric efficiency (VE), resulting in a brake thermal efficiency (BTE) reduction [11]. Then, to solve this issue the air-fuel ratio (λ) is fixed looking for the optimal performance of the engine which together with the technical advances in H_2-ICEs, it has recently been achieved similar power outputs to commercial gasoline and diesel-fuelled engines. In this sense, the stoichiometric air-fuel ratio (λ_{st}) which means the amount of air required for the amount of fuel, is quite lower than the amount required for gasoline and diesel, due to its higher reactivity, reducing fuel consumption. According to the wider flammability range, it could derive in backfire and pre-ignition abnormalities,

producing explosions in the intake manifold, which are avoided working at the optimum injection timing and Spark Advances (SA). Thus, the wider range allows higher engine efficiency than conventional fuels [12]. On the other hand, H_2 is characterised by a higher laminar flame speed (S_L). Thus, as the H_2 concentration in the fuel increases, the SA angle decreases because of higher S_L improving the mixture chemical reactivity and reducing the combustion duration [13]. Finally, the autoignition events of unburned gases can take place without the participation of any ignition source, promoting the formation of knocking [11]. In such a way, despite the higher autoignition temperature of H_2, its lower energy required to ignite makes it more prone to auto-ignite [14]; nevertheless, these events are easily controlled throughout the load [12].

1.3. Internal Combustion Engine.

1.3.1. Internal Combustion Engine (ICE).

Overall, the main objective of internal combustion engines can be defined as the production of mechanical power from the chemical energy contained in the fuel [15]. In this kind of engines, the energy is released by the oxidation of the fuel that is fed into the combustion chamber. Then, the ignition can be carried out in two different ways: spark-ignition (SI) and compression-ignition (CI). The SI engines are also called Otto engines or gasoline engines, and similarly, the CI engines are also called diesel engines. The ICEs in transportation devices usually works under a four-stroke cycle which means that four strokes are required to complete one engine cycle. Each stroke is called differently according to its function, so the engine cycle is composed of the strokes that are represented below in Figure 1.4 [15].

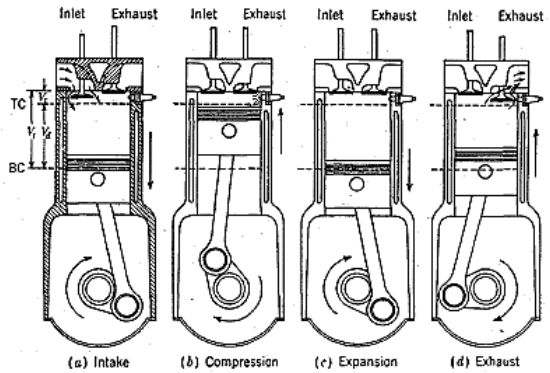

Figure 1.4. Four-stroke cycle engine [15].

In that way, according to this figure the engine cycle is composed by [15]:

- Intake: During this stroke, the intake valves are opened, and the piston goes down while air or air-fuel mixture, depending on the injection strategy, enters the cylinder. Intake stroke finished in the Bottom Dead Centre (BDC) position of the piston.
- Compression: It starts when the intake valves are closed, and the piston ascends compressing the mixture that entered during the Intake stroke. Compression stroke ends in the Top Dead Centre (TDC) position of the piston.
- Combustion and expansion: Combustion begins applying an electrical spark (gasoline engine) or using high-pressure fuel injection systems that auto-ignites in the hot compressed gas (diesel engine). The own combustion reaction forces the piston to go down and delivers work in terms of energy, because it is an exothermic reaction, to the crankshaft through the expansion of the hot gases.
- Exhaust: Finally, when the exhaust valves are opened, the piston goes upwards again for the exhaust stroke, ejecting the burned or exhaust gases.

1.3.2. Hydrogen-powered Internal Combustion Engine (H_2-ICE).

The Spark-Ignition engines are going to be the subject of this study because this kind of engines is easier to adapt into an H_2-ICE. The parameter that provides the highest influence and enables to control fuel behaviour, is the air-fuel ratio (λ), which is usually fixed to control the combustion events, especially in H_2-ICEs because of the impact on the efficiency of the engine. Then, due to the special properties of the H_2, as a first approach, the firsts H_2-ICEs mostly used a port fuel injected (PFI) design, giving a lower power density than gasoline. Hence, some advances have been made to improve power densities. Thus, the two main injection strategies are explained below and depicted in Figure 1.5 [16]:

- Port fuel injected (PFI): The fuel is injected into the intake manifold, premixing the fuel, in this case, H_2, with the air which flows up to the intake valves. This kind of injection configuration is the most used because it is the easiest way for adapting the ICEs into the H_2-ICEs. Nowadays, in H_2-ICEs with PFI, regarding the

Nitrogen Oxides (NOx) formation, a correlation with λ has been found, employing a lean constant λ strategy, and then replacing the gasoline fuel system with hydrogen injectors or cryogenic hydrogen port injection. Therefore, the improvements in the injection step suppose an increase in the power output, allowing working at lower λ constant values without compromise the levels of NOx emissions [16].

- Direct injection (DI): The fuel is directly injected into the combustion chamber, so the air and fuel are mixed and react at the same time. This kind of injection would be useful to avoid some problems derived from the high LHV and low density of H_2, increasing the pressure of the fuel gases [13]. Currently, to increase the power output, this configuration made some changes related to the injection timing such as multiple injection strategies with two or more injection pulses per cycle which is the best strategy found at high loads. However, due to the shortest time on each injection, multi-injection strategies must provide high-pressure levels and injection flow rates, limiting their application to low engine speeds [17].

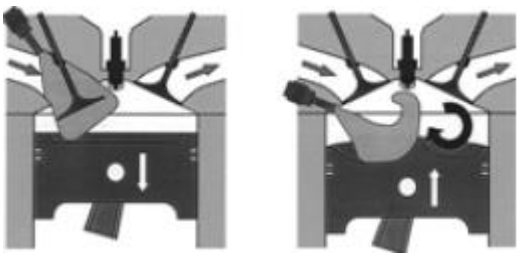

Figure 1.5. PFI (On the Left) and DI (On the right) injection strategies [17].

1.3.3. Advanced H_2-ICEs: Hydrogen-Methane blends.

The main environmental drawback of using H_2 as fuel is the generation of specific emissions of nitrogen oxides (sNOx) when is running at high engine loads. Hence, to reduce the emissions of sNOx generated during the combustion, blends of H_2 and CH_4 could be a feasible solution. The main features from the H_2 - CH_4 blends are:

- The mixture H_2 - CH_4 allows to work with a wider range of λ values, resulting in higher power performances [11].

- As a drawback, CH_4, which reduces the emissions of thermal NOx, also increase the amount of CO_2, CO, and hydrocarbons (HC), and at the same time reduce the BTE, the S_L and the flammability ranges [11].

1.4. Valorisation of residual streams from industry: Coke oven gas

Another useful way to promote the circular economy in Europe, is the valorisation of residual streams from industry, to turn them into valuable products [18], such as the Coke Oven Gas (COG) which is extracted from the residual streams of coke manufacture and subsequently purified by Pressure Swing Adsorption (PSA). Furthermore, it is important to highlight that is constituted of some components that can be used as fuels. As can be seen in Table 1.2 [19]:

Table 1.2. Composition (vol%) of COG residual stream from industry [19].

COG constituents	Vol%
H_2	55 – 60
CH_4	23 –30
CO	5 – 8
CO_2	1 – 2
N_2	3 – 6
C_2H_4	1 - 1.5
C_2H_6	0.5 - 0.8
C_3H_6	< 0.07
H_2S	< 3.2 x 10^5

According to Table 1.2, the composition of COG is based on a H_2 - CH_4 blend. Therefore, COG can be used as fuel for ICEs. In this sense, the COG has intermediate properties, in comparison with H_2 and CH_4, as can be seen in Table 1.3 [11].

Table 1.3. Typical physicochemical properties of H_2, CH_4 and COG at 273.15 K and 10^5 Pa (STP) [11].

Gas	H_2	CH_4	COG
LHV (MJ/kg)	120.00	50.00	39.85
LHV (kJ/mol)	241.91	802.12	395.5
LHV (MJ/m^3)	9.92	32.91	16.23
Density (kg/m^3) at STP	0.08	0.66	0.41
Molecular weight (g/mol)	2.02	16.04	9.92
Stoichiometric ratio (λ_{st})	34.21	17.20	12.72
Flammability range (vol%)	4.00-75.00	5.30-15.00	4.40-34.00
Laminar flame speed (m/s)	2.85-3.25	0.38	0.68-0.88

Based on the values collected in Table 1.3, it can be determined that COG combines the advantages of both; CH_4 and H_2, allowing the extension of the λ factor, from 1 to 2. In addition, it is important to highlight the good knocking resistance of COG, given by the CH_4 contained in the mixture, allowing the variation of the λ factor, without experimenting any abnormal combustion phenomena.

1.5. Background.

This work is part of the European project HYLANTIC EAPA_204/2016 "The Atlantic Network for Renewable Generation and Supply of Hydrogen to promote High Energy Efficiency", coordinated by the Department of Chemical and Biomolecular Engineering of the University of Cantabria. Thus, this study is based on the design and simulation of an ICE adapted to be fuelled by H_2, studying the main strengths and weaknesses of H_2, and considering the use of other alternative fuels as CH_4 and COG. In this sense, according to the current sustainability goals, also shorted in the transport sector, it is one of the main pillars to achieve the transition towards carbon neutrality.

Then, due to the current trend in the EU which is being driven towards a circular economy as part of the sustainable development. The improvements in technology, involving transport mobility, are predestined to be crucial in the achievement of a critical reduction of atmospheric emissions, specially, CO_2, HC, and NOx emissions.

In this sense, H_2-ICEs will lead the new mobility horizon, making the road transport more preservative with the environment, adapted to the necessities of customers and economically viable.

1.6. Objectives.

The main goal of this work is modelling an internal combustion engine powered by H_2 and compare it with another alternative fuels. To achieve it, the following objectives should be fulfilled:

- Spark engine suitable geometric design, meshing and export to the simulation tool ANSYS Forte.
- Simulation of Hydrogen combustion, just as the alternative fuels.

- Study of the influence of the engine speed (rpm) and the Air-Fuel ratio (λ) variables on engine performance and emissions.
- Comparison of engine performance results in Hydrogen simulations, according to the temperature, pressure and emissions. In addition to the comparison of engine performance results in Hydrogen, Methane and Coke Oven Gas simulations.

2. Methodology: ANSYS Forte.

First, in this study a naturally aspirated four-cylinder Volkswagen Polo 1.4 L SI-PI ICE is going to be reproduced, with a Compression Ratio (CR) of 10:5:1 [11], originally run-on gasoline, which was adapted to be fuelled by H_2, being a generic car representative of small vehicles widely used for both city and interurban traffic. The main changes to convert the Otto-engine, into an H_2-ICE, are mostly related to the H_2 feeding system, for instance, the plastic material of the inlet manifold was changed by a cast manifold, preventing backfire complications and the conventional gasoline injectors are replaced by specific H_2 injectors [20]. Then, based on the specifications of the original engine, and the data provided, the geometrical model of the engine was made.

In that way, the procedure to be followed in order to perform the H_2-ICE model and simulation, starts importing the geometrical design to the simulation software workbench. Then, its geometrical meshing is performed to refine and import the geometric data in the Computational Fluid Dynamics (CFD) software in which another meshing is applied, but in this case, the meshing is oriented to the engine simulation parameters and the refining of the simulation performance. Finally, in the CFD software, a wide variety of parameters and features must be defined before simulating, including these meshes, the chemical reaction inside the combustion chamber, the timing in the spark and the fuel injection.

To do this, a very well-known engineering software was used: ANSYS 2020 R1®. In that way, access to its tools is possible thanks to the simulation software package called ANSYS Workbench 2020 which contains the packages that are going to be used:

- ANSYS SpaceClaim: This is a Computer-Aided Design (CAD) for manufacturing.

- ANSYS Meshing R2 2020: Used to create the geometrical meshing and refine it into a first approach.
- ANSYS Forte: The CFD software that oversees the simulation.

2.1. Geometric design and Meshing.

First, the geometric design was previously developed by using Autodesk Inventor, and then the piece has been imported to ANSYS. In ANSYS Workbench, the engine model has to be imported and opened in SpaceClaim®, then to Mesh®, in order to make the proper meshing for the refinement of the geometric details, and lastly, this meshing is imported into ANSYS Forte. For this reason, the different steps to import in ANSYS have been explained in Annex A.I.

Following with the geometry imported in SpaceClaim®, it is important to identify the different parts that compose the engine, which can be seen in Figure 2.1.

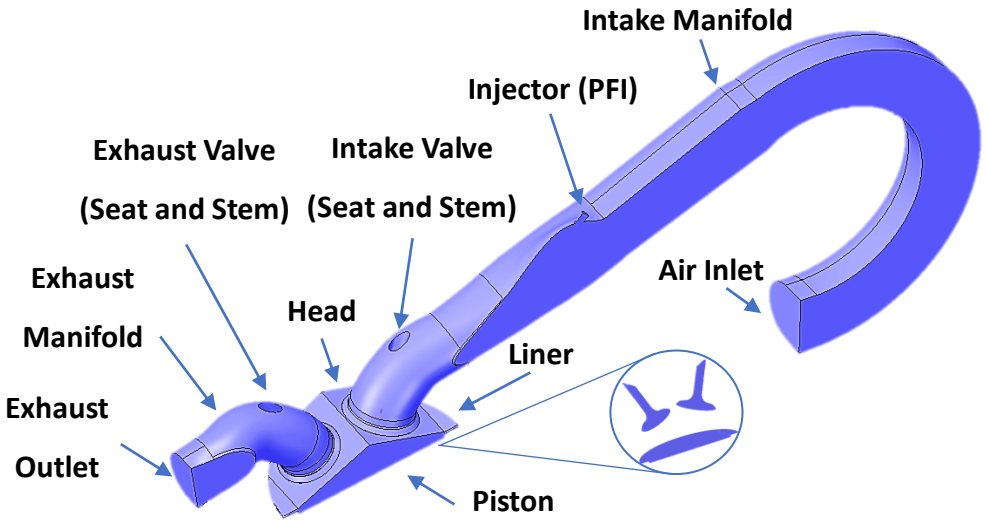

Figure 2.1. The geometric design of the internal combustion engine.

The designed engine has been simplified to the symmetric side of just only one of the four cylinders from the entire H_2-ICE because every cylinder is equal to the other. Therefore, the aim of using the symmetry of one cylinder is the reduction the time required to carry out the simulation. Then, after defining the different parts of the geometry, it is imported in Mesh®, to perform the meshing according to Annex A.II.

In that way, the meshing tool aims to create the most accurate mesh, considering the simulation time involved in very precise meshing. For this reason, Table 2.1 collects the

refinements applied to the geometric mesh, overwriting the general mesh that is assigned to the entire solid.

Table 2.1. Refinements and overall mesh applied to the model in Mesh®.

Element	Scope method	Number of faces / Named selection	Size element	Other features
Engine	Overall Mesh	All the solid	$2.50 \cdot 10^{-3}$	"Hydrodynamics" (physics reference)
Injector	Geometry selection	2 Faces	$5.00 \cdot 10^{-4}$	-
Piston	Geometry selection	11 Faces	$1.00 \cdot 10^{-3}$	-
Manifolds	Geometry selection	2 Faces	$1.50 \cdot 10^{-3}$	-
Valve Seats	Named selection	"ValveInSeat" "ValveOutSeat"	$1.50 \cdot 10^{-3}$	-
Symmetry	Geometry selection	5 Faces	$1.50 \cdot 10^{-3}$	“Capture Curvature”

2.2. Simulation software: ANSYS Forte.

ANSYS Forte is the CFD code software employed to carry out the simulation. Therefore, there are a lot of parameters that must be defined, calculated, expressed by default and created. In that way, the first task to do was performing the simulation meshing, defining the material point where the simulation takes place and the global mesh size of the model. Then, for every geometry element, one different surface refinement and another point refinement in the region of the spark were created. In that way, it is important to note that the walls were refined to improve the heat transfer during the combustion reaction and were applied extra refinements when the piston reaches the TDC that occurs two times during the engine cycle, especially in the compression stroke. After that, a similar form as the geometrical mesh appears, which can be seen in Figure 2.2.

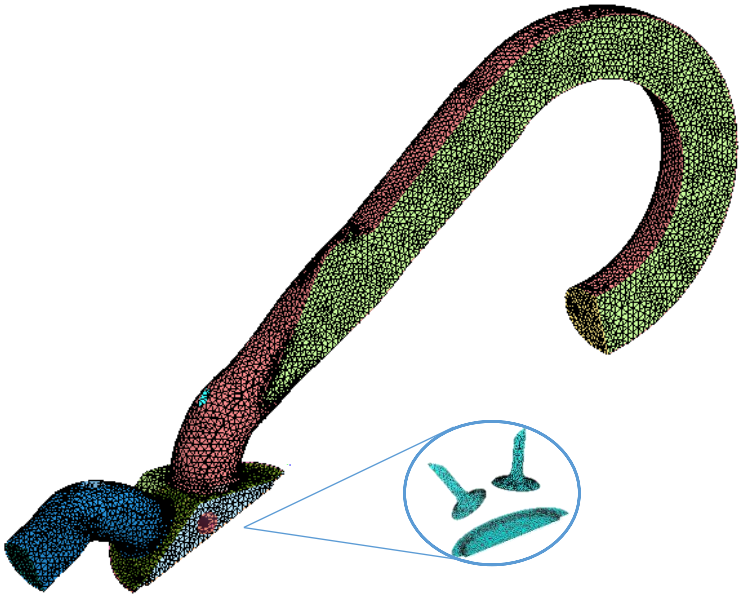

Figure 1.2. ANSYS Forte simulation model.

Afterwards, the chemistry of the combustion reaction for H_2, CH_4 and COG were introduced, which are going to be the different fuels employed for the simulations, especially H_2. Hence, the chemical reaction mechanism has to be imported. In this sense, it is crucial to find out a mechanism that faithfully represents combustion of H_2, CH_4 and COG, because all the results depend on the correct development of the combustion. For this reason, the most complete mechanism GRI-Mech 3.0 was imported. It works in a good way with H_2, but also with CH_4, including all its possible reactions and COG that can be defined as a mixture based on Table 1.3, being a complete mechanism. This mechanism was developed by the University of California, Berkeley, and contains 325 reaction and 53 species [21].

After that, the spark was also defined. In order to calculate the spark duration, the engine speed (rpm) is decisive. Moreover, it is important to consider the reference data that is used by ANSYS Forte:

$$Nominal\ spark\ angle = 720^{\circ}$$

$$Duration = 1\ ms$$

Based on this reference, the duration is obtained following Eq.1.

$$Duration\ (^{\circ}) = Engine\ Speed\ \left(\frac{rev}{min}\right) \cdot \frac{1\ rev}{60\ s} \cdot \frac{360^{\circ}}{1\ rev} \cdot 1\ ms\ \cdot \frac{1 \cdot 10^{-3}\ s}{1\ ms} \qquad (Eq.1)$$

However, in the case of the SA, measured in degrees Before Top Dead Centre (dBTDC), it is related to the kind of fuel used and the λ ratio for each case. The results of the

spark duration and the optimum SA employed, according to the engine speed and the λ ratio have been collected in Table 2.2.

Table 2.2. Spark Advance (SA) and duration of the spark for every simulation.

Fuel	Lambda (λ)	Engine Speed (rpm)	Spark Advance (dBTDC)	Duration (°)
H_2	1.5	2000	10	12
H_2	1.5	3000	10	18
H_2	1.5	4000	15	24
H_2	1.5	5000	15	30
H_2	2	3000	25	18
CH_4	1.5	3000	60	18
COG	1.5	3000	25	18

As can be seen, the lower the λ ratio and the higher the reactivity of the fuel, the lower the SA required to obtain the optimum SA, due to the higher fuel concentration, increasing the S_L, operating with Wide Open Throttle (WOT) loads and the optimum SA to obtain the Maximum Break Torque (MBT). Finally, in the case of the spark duration, it increases with the engine speed.

To perform a suitable simulation, it is important to set the boundary conditions, depending on the location of the geometry elements, the boundary system can be referred to as the inlet, outlet, or wall boundaries, apart from the symmetry boundaries that are just related with the surfaces of the cross-section of the model. Thus, beginning with the inlets which are the "Air Inlet" and the "Fuel Inlet", the main parameters of "Air Inlet" have been collected in Table 2.3.

Table 2.3. Air Inlet critical boundary conditions: Pressure and Temperature.

Air Inlet		
Speed (rpm)	Pressure (bar)	Temperature (K)
2000	0.92	314
3000	0.91	311
4000	0.89	309
5000	0.88	307

To explain briefly the effect of these parameters in the engine performance, in the case of the "Air inlet" it is important to highlight the pressure and temperature effects related to the engine speed. In the case of the pressure, the higher the engine speed,

the lower the pressure used to feed the intake manifold, because when the speed is higher, the piston creates a vacuum inside of the cylinder, reducing the pressure in the manifold. In the case of the temperature, when the engine speed increases, the temperature in the air intake decreases in the same way that pressure does, because the higher flow velocity of the air, the lower the residence time inside of the cylinder, and hence, the air does not have enough time to warm up.

On the other hand, the second inlet boundary condition is the "Fuel Inlet" which corresponds with the injection of the fuel. Therefore, it was required to create the velocity profile of the fuel, which is represented as a pulse function. The desire velocity profile is obtained throughout the calculation of the injection velocity and the Pulse Width (PW) which represents the range of Crank Angles (CA) in what the injection takes place with constant velocity, supposing a constant injection pressure of 3 bar. The injection velocity and the PW are obtained from eq. 2 and 3.

$$v_i\left(\frac{m}{s}\right) = \frac{\dot{m}_i\ \left(\frac{g}{s}\right)}{\rho_i\ \left(\frac{g}{cm^3}\right) \cdot A(cm^2) \cdot 100\left(\frac{cm}{m}\right)} \qquad (Eq.2)$$

$$PW\ (°) = \frac{N\ \left(\frac{°}{s}\right)}{\dot{m}_f\ \left(\frac{g}{s}\right)} \cdot m_{full}(g) \qquad (Eq.3)$$

In the case of the injection velocity (v_i), it varies depending on the fuel composition, because of the variation of the mass flow and injection density of each fuel (ρ_i), according to the calculations explained in Annex B.II.

On the other hand, the total mass of fuel (m_{full}) was obtained from the assumption of the introduced air mass quantity, in terms of oxygen (m_{O_2}), and the subsequently calculation of the relative lambda (λ_{Rel}), the λ_{Est} and the actual lambda (λ_{actual}), according to the following eq. 4.

$$\lambda_{Rel} = \frac{\lambda_{Actual}}{\lambda_{Est}} = \frac{\left(\frac{\dot{m}_{Air}}{\dot{m}_{Fuel}}\right)_{Actual}}{\left(\frac{\dot{m}_{Air}}{\dot{m}_{Fuel}}\right)_{Est}} \qquad (Eq.4)$$

In addition, the calculations employed to obtain the λ ratio and all the parameters needed for the PW, including itself, are explained in detail inside Annexes B.I and B.III, and their velocity profiles have been represented in Annex C.I from Figure C.1 to Figure C.7. Moreover, the fuel composition is defined in mole fraction, varying according to the kind of fuel used (H_2, CH_4 or COG). The values of the assumptions m_{O_2}, and the results of the m_{full} and the PW for each fuel, are shown in Table 2.4.

Table 2.4. Mass of fuel injected, and PW results obtained from the mass of oxygen (O_2) assumed.

H_2				
RPM	λ_{Rel}	m_{O_2} (mg)	m_{full} (g)	PW (°)
2000	1.5	54.5	0.0046	94
3000	1.5	58.5	0.0049	149
4000	1.5	62.5	0.0053	212
5000	1.5	65.55	0.0055	277
3000	2	62.5	0.0039	120
CH_4				
RPM	λ_{Rel}	m_{O_2} (mg)	m_{full} (g)	PW (°)
3000	1.5	69.5	0.0116	107
COG				
RPM	λ_{Rel}	m_{O_2} (mg)	m_{full} (g)	PW (°)
3000	1.5	64.2	0.0145	189

Then, apart from the values applied in the inlet system boundaries, the outlet system is composed by just only one boundary condition, the "Exhaust" condition, taking care mostly of the control in the outlet pressure, that must be atmospheric.

Finally, the boundary conditions of the wall systems, have a strong dependency on the wall temperature, because it is very closely related to the heat transfer phenomena. In that way, the values defined in the simulations appear below in Table 2.5.

Table 2.5. Walls Boundary Conditions: Wall Temperature.

Boundary Condition	Temperature (K)
Piston	500
Head	400
Liner	400
In Valve	400
Out Valve	550
Intake Manifold	313
Exhaust Manifold	500

The “In Valve” and the “Out Valve” also have a type of motion that requires the implementation of one lift profile for each one, because they are constantly opening and closing, that represents the distance versus the CA, and can be seen in the Annex C.II.

Proceeding with the definition of the initial conditions to carry out the simulation, it is important to know that the engine is composed of three regions; the intake, the cylinder, and the outlet, so every region has some initial conditions to initialize the simulation. In this sense, it is needed to import the composition inside of the cylinder, which is the same as in the exhaust manifold, to do this, exists one tool called “Composition Calculation Utility”. However, to carry out the calculation of its composition, it is required to calculate the exact fuel mass injected ($m(mg)$) which is the same as the m_{full}, previously calculated to obtain the PW, in milligrams, and it can be calculated using the following eq. 5.

$$m\,(mg) = \frac{1^\circ}{N\left(\frac{^\circ}{s}\right)} \cdot \sum_{n^\circ} \dot{m} \qquad (Eq.5)$$

$$m\,(mg) = \frac{1^\circ}{N\left(\frac{^\circ}{s}\right)} \sum_{n^\circ} \left(v\left(\frac{m}{s}\right) \cdot \rho\left(\frac{g}{cm^3}\right) \cdot \frac{10^6 cm^3}{1m^3} \cdot A(cm^2) \cdot \frac{1m^2}{10^4 cm^2} \cdot \frac{10^3 mg}{g} \right) \qquad (Eq.5)$$

The aim of recalculating the mass of fuel injected throughout this formula, is to obtain the most accurate result and check that the previous calculation has been properly performed. Afterwards, to obtain the total mass injected, it is required to multiply by two because the symmetry has already considered in the symmetric injector area (A) that appears in this equation and the calculations of the injection velocity (v). For this reason, the mass obtained for each simulation has been collected in Table 2.6, found the same values have been obtained for the total mass injected during the PW in milligrams.

Table 2.6. Checking of the mass of fuel injected during the PW.

Gas	**H_2**					**CH_4**	**COG**
λ_{Rel}	1.5				2	1.5	1.5
RPM	2000	3000	4000	5000	3000	3000	3000
m (mg)	4.606	4.906	5.260	5.510	3.937	11.671	14.550

Finally, the equivalence ratio (ϕ) is introduced, which is calculated as can be seen in Eq. 6.

$$\phi = \frac{1}{\lambda} \qquad (Eq. 6)$$

Subsequently, the duration of the simulation was defined as being based on the CA. In this sense, the Initial CA was assigned to one value of 200°, which is suitable for all over the simulations and then the Final Simulation CA was calculated to reach four-engine cycles, as can be seen in Eq. 7.

$$Final\ Simulation\ CA = Initial\ CA + One\ Cycle \cdot Number\ of\ Cycles \qquad (Eq. 7)$$
$$Final\ Simulation\ CA = 200\ ° + 720 \cdot 4 = 3080\ °$$

Once the simulation is done, the results can be contrasted according to the λ_{Rel}, which is the desired ratio, performing an iterative process that has been explained in Annex A.III.

Finally, before running the simulation is possible to choose the number of cores, in MPI Args, that the computer can virtually provide. In this study, simulations were carried out with MPI solver in a workstation property of the department, with two processors Intel® Xeon® Gold 6148 of 20 physical cores each one, and 256 GB RAM. Connection to this workstation was established with remote access through the local network, selecting the number of cores (MPI Args) desired to perform faster the simulations.

2.3. Simulation plan

The simulation plan is an important part of the methodological process in modelling and simulation studies. The simulation plan consists of the more exhaustive study on H_2-ICEs and includes the simulations of CH_4 and COG as fuels, to compare their performances. Then, there are two main parameters that are going to be fixed as operational conditions with different values for each simulation that affect considerably the SA, the injection velocity, and the PW, which in turn wields control in the engine performance. Those parameters are the λ and the engine speed. Finally, the simulation plan has been exposed in Table 2.7.

Table 2.7. Simulation plan.

Gases	Relative Lambda (λRel)	Engine Speed (rpm)	Spark Advance (SA) (dBTDC)	Injection velocity (v) (m/s)	Pulse Width (PW)	End of Injection (EOI)
H_2	1.5	2000	10	275	94	485
		3000	10		149	490
		4000	15		212	495
		5000	15		277	500
	2	3000	25		120	490
CH_4	1.5	3000	60	115	107	490
COG	1.5	3000	25	130	189	490

The End of Injection (EOI) is a key parameter, and their values are based on the recommended upper limits for the PW on each specific operational condition, that have been chosen in order to avoid the accumulation of fuel residues in the intake manifold [22]. Therefore, these values represent the desirable time in which the injection pulse must stop. On the other hand, the lower limit is established depending on the PW and the required EOI. Finally, the SA and the injection velocity are shown in Table 2.7 which have a strong influence in the PW and in the engine performance.

3. Discussion of the Results

Based on the previous methodology and calculations already explained, this section describes the results obtained for each simulation, following the simulation plan.

3.1. Hydrogen.

There are some important results that must be covered to describe in a good way the behaviour and the performance of the H_2-ICE. Global power output values, for instance, the power, are represented by a single value. Conversely, other variables have a dependency to the CA, such as temperature, pressure, and NOx emissions, and hence, vary with it.

Finally, it is important to highlight that all the cases are based on the λ and the engine speed, values and they have been plotted within the last cycle of the engine, which is the fourth, to obtain results that fit better with the real values.

3.1.1. *Influence of the rpm and the Air-fuel ratio.*

The engine speed and the λ factor, exert a strong influence on the parameters that give the necessary information to describe the performance of the H_2-ICE. In that way, the CA has been trimmed considering the time at which the combustion occurs, because it is the moment in what the chemical reaction is carried out and the power is delivered to the engine, which turns that chemical energy into mechanical energy.

In this sense, for the H_2 simulations, which are the backbone of this study, Figures 3.1, 3.2 and 3.2, have been depicted.

- Temperature (K) vs CA (◦):

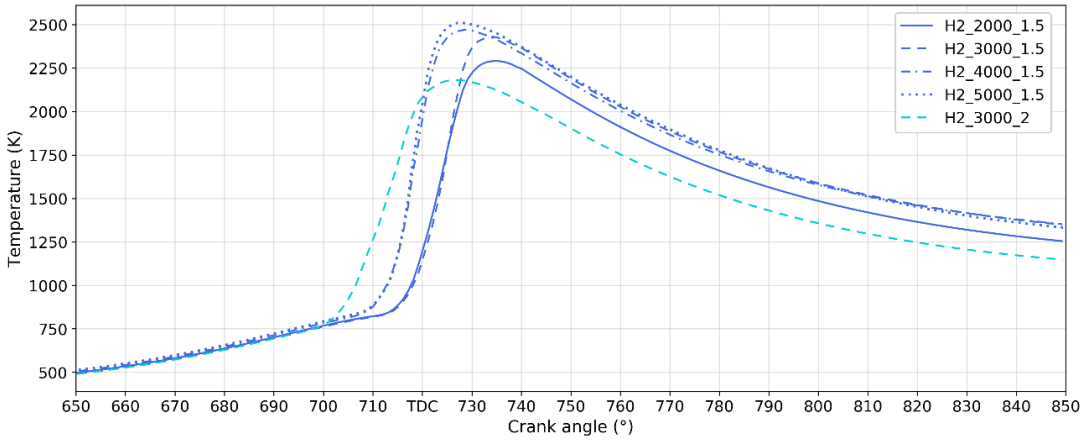

Figure 3.1. Temperature vs. CA for different engine speeds (rpm) and λ ratios in H_2 simulations.

In this figure, the relationship between the temperature (K), the λ factor (-) and the engine speed (rpm) of H_2 has been depicted, finding that for each engine speed and λ factor values, all the simulations follow the same trend.

At the beginning, when the compression stroke is approaching to the TDC, the spark plug ignites at different CA depending on the engine speed, the λ factor and the fuel composition which in this case is just H_2. These advances in the spark ignition are reflected in the CA at which the slope changes before reaching the maximum. In this sense, the figure shows the necessity of increase SA mainly when the λ factor is higher (λ=2) because the air-fuel mixture becomes leaner due to the reduction of the concentration of H_2, thus reducing the reactivity of the mixture, and hence, requiring more time to ignite. Furthermore, the difference in the engine speed also implies a change in the ignition timing, in this case, when the engine is working at 2000-3000

rpm, the SA is delayed comparing to the 4000-5000 rpm, and hence, the peak of temperature is reached later. In that way, similar results in the case of 4000-5000 rpm were observed, but between 2000-3000 rpm the largest temperature difference occurs, due to the higher amount of fuel injected, increasing the PW when the engine speed increases.

Thus, regarding to the maximum combustion temperature, the higher the engine speed, the higher the temperature, and conversely, the higher the λ factor, the lower the temperature. For this reason, increasing the λ factor up to λ=2, the temperature profile becomes smoother and although its SA is higher, it is quickly surpassed by the simulations with lower λ, even in the case of 2000 rpm at λ=1.5, despite working at lower engine speed, it achieves a higher temperature. Therefore, the effect of the λ factor, in the case of H_2, exerts a stronger influence on the temperature than the engine speed.

Lastly, after reaching the TDC, during the expansion stroke while the piston is going closer to the BDC, the temperature inside of the cylinder is reduced, due to the pressure reduction and the heat transfer through the walls.

- Pressure (bar) vs CA (◦):

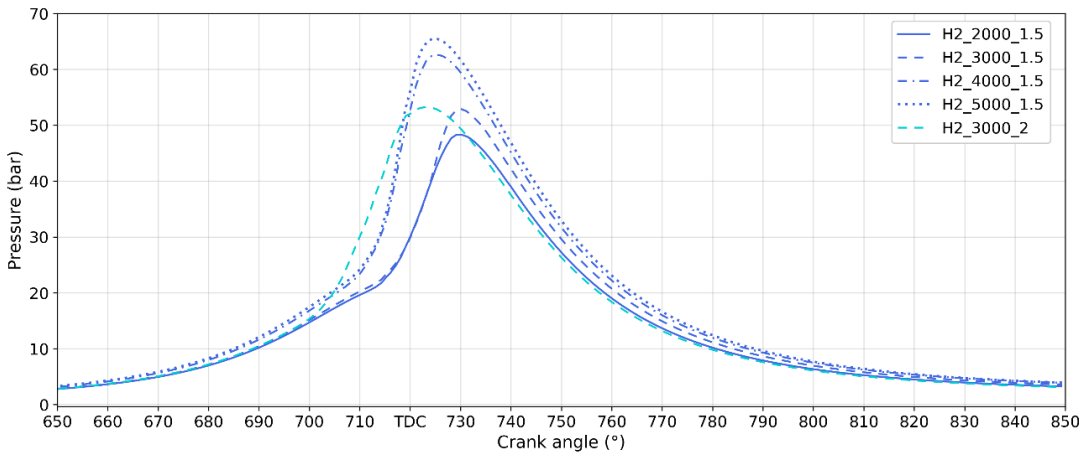

Figure 3.2. Pressure vs. CA for different engine speeds (rpm) and λ ratios in H_2 simulations.

First of all, it is important to note that H_2 and all the fuels assessed in this study are gases, so they are more sensitives to changes in pressure than liquid fuels. Although this pressure profile, compared to the temperature profile is more like an impulse function, the pressure, as the temperature, increases with the engine speed. Initially,

the pressure increases with the reduction of the volume experimented inside the cylinder because of the compression stroke and then, once the peak of pressure is reached, it remains slightly because the temperature is still increasing.

Furthermore, it should be also affected by increasing the λ factor when operates at higher values (λ=2), due to the lower concentration of H_2 in the mixture that would reduce the peak of pressure because less heat is released in the combustion. However, both different λ (λ=1.5 and λ=2), at the same engine speed (3000 rpm), have the same pressure values, because of the SA causes the pressure rising, so it is more sensitive to the changes in SA.

Therefore, the relation among the temperature and the pressure, and their dependency on the operating conditions, makes it possible to determine the optimum operating conditions, at the optimum SA.

- NO emissions (ppm) vs CA (◦):

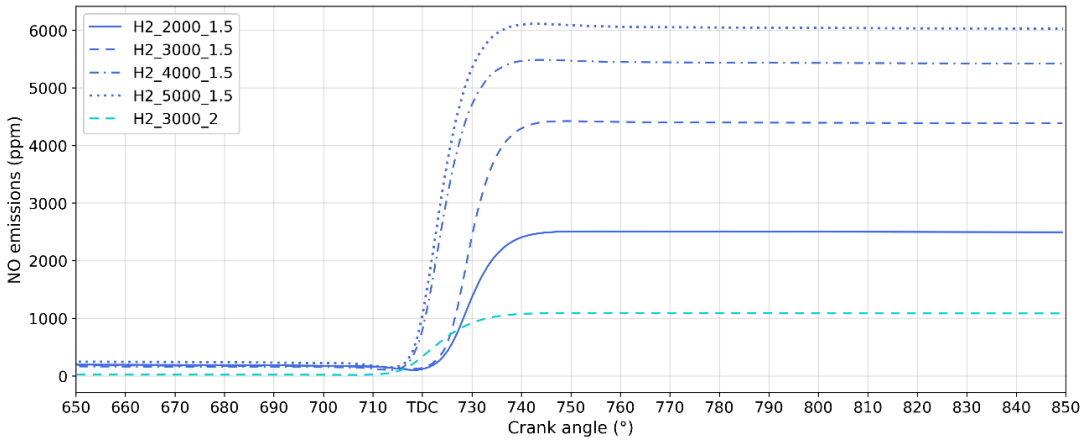

Figure 3.3. NO emissions vs. CA for different engine speeds (rpm) and λ ratios in H2 simulations.

One of the most important parameters in H_2-ICEs is the control of the NOx emissions to the atmosphere because the NOx, which in this case is mostly Nitrogen Monoxide (NO), is the only pollutant related to H_2 combustion. However, the amount of NOx emitted in H_2-ICEs is still quite low.

According to this figure, the increase in the λ, using a λ=2 factor, suppose a drastic reduction in the amount of NOx, resulting in 1000 ppm of NO, making a smoother curve than the simulations with λ=1.5 during the combustion stroke, since increasing the combustion temperature, according to the extended Zeldovich reaction model, the

rate of NOx production in the reaction increases as well. On the other hand, increasing the engine speed, the amount of NOx emitted increases, due to the higher temperatures reached during the combustion. For this reason, there is a problem in achieving the reduction of NOx formation, without reducing engine performance too much; notwithstanding, it is possible to do this, by means the optimum SA, modifying the operating conditions.

Finally, after the combustion reaction takes place, during the expansion stroke the amount of NOx in the combustion chamber remains stable, because there is no further generation of NOx as they are only generated in the reaction, and despite the great difference among the simulations shown in this figure these differences are not very big, because the NOx emissions are being measured in ppm.

In addition, the relationship between the engine speed with the temperature, pressure and NO formation as well as the mole fraction of fuel during the injection were also assessed throughout some three-dimensional figures, in a certain CA, previously selected, as can be seen in Annex C.III.

Based on the results of temperature, pressure and NOx emissions obtained in these simulations, the main parameters related to the engine performance have been calculated and are shown in Table 3.1.

Table 3.1. Engine Performance and emissions results obtained in Hydrogen simulations.

Cycle 4	Power (kW)	Torque (Nm)	BMEP (bar)	BTE (%)	BSFC (g/kWh)	EV (%)	CHR (J)	sNO (g/kWh)
H_2: 2000 rpm λ=1.5	3.31	15.81	5.72	37.94	79.08	62.58	517.04	14.05
H_2: 3000 rpm λ=1.5	5.27	16.77	6.07	35.65	84.15	64.14	582.05	23.91
H_2: 4000 rpm λ=1.5	6.94	16.56	5.99	32.87	91.28	70.09	622.2	32.35
H_2: 5000 rpm λ=1.5	8.25	15.76	5.70	29.83	100.56	71.48	652.01	38.76
H_2: 3000 rpm λ=2	4.21	13.40	4.85	35.51	84.49	67.79	469.11	7.57

According to this table, the higher the engine speed, the higher the Power, Brake Specific Fuel Consumption (BSFC), Volumetric Efficiency (VE or η_e), Chemical Heat

Release (CHR) and specific Nitrogen Oxides (sNOx), because they are directly related. However, the lower the Brake Thermal Efficiency or fuel conversion efficiency (BTE or η_f), due to the increase in BSFC. As can be seen in eq. 8.

$$\eta_f = \frac{W_c}{m_f \cdot Q_{HV}} = \frac{\left(\frac{P \cdot \eta_R}{N}\right)}{\left(\dot{m}_f \cdot \frac{\eta_R}{N}\right) Q_{HV}} = \frac{1}{BSFC \cdot Q_{HV}} \qquad (Eq. 8)$$

Where Q_{HV} is the Volumetric LHV (MJ/m^3).

On the other hand, the Torque, and the Brake Mean Effective Pressure (BMEP) fluctuate depending on the engine speed. In this sense, the higher the engine speed, the higher the peak of pressure during the combustion, and hence, the temperature increases as well. This increase in the peak of pressure provides a higher Power (P) whose relationship can be explained through equations 9 and 10.

$$P = \frac{W_{c,i} \cdot N}{\eta_R} \qquad (Eq. 9)$$

$$W_{c,i}\ (J/Cycle) = \oint p \cdot dV \qquad (Eq. 10)$$

Where η_R is the number of crank revolutions for each power stroke per cylinder ($\eta_R = 2$), $W_{c,i}$ Is the work delivered per cycle (J/Cycle) and N Is the engine speed (rev/s).

Therefore, there is a direct relationship between engine speed and power, and then, the power and the pressure (p) are related by means the work delivered per cycle ($W_{c,i}$).

In turn, the Torque (N·m) is directly related to the Power (kW) delivered, because it is defined as the external force multiplied by the distance between its application point and the axis, in this case, the crankshaft. Hence, is related to the amount of energy that the spin of the crankshaft can turn into mechanical energy, which is converted into electrical energy. However, it is inversely proportional to the engine speed (N), as can be seen in eq. 11.

$$P(kW) = 2\pi NT * 10^{-3} \qquad (Eq. 11)$$

Finally, the Brean Mean Efficiency Pressure (BMEP), is described by eq. 12, which in the same way as the Torque it is directly related to power and inversely proportional to the engine speed (N).

$$BMEP\ (bar) = \frac{P \cdot \eta_R}{V_d \cdot N} = \frac{W_{c,i}}{V_d} \qquad (Eq. 12)$$

Where; V_d is the cylinder volume displaced by the piston in all the cylinders (dm^3).

For this reason, both parameters have a maximum between 3000 and 4000 rpm, which are intermediate engine speed values since the positive effect of power is balanced by the reducing effect of engine speed.

Afterwards, although the increase in the Power, decreases the sNOx emissions, according to eq. 13.

$$sNOx(g/kWh) = \frac{\dot{m_{NOx}}}{P} \qquad (Eq. 13)$$

Where; $\dot{m_{NO_x}}$ is the mass flow of NOx produced during the combustion (g NOx/h).

In Table 3.1, the results obtained shows that the sNOx increases even if the Power increases. Therefore, the $\dot{m_{NO_x}}$ increases with the engine speed because of the temperature rising, more than Power does.

In this sense, as the temperature rises with the engine speed, the CHR rises as well, because of the exothermic character of the combustion reaction, increasing the combustion efficiency (η_c), as can be seen in equations 14 and 15.

$$Net\ CHR\ (J) = H_R(T_A) - H_P(T_A) \qquad (Eq. 14)$$

$$\eta_c = \frac{(H_R(T_A) - H_P(T_A))}{m_f \cdot Q_{HV}} \qquad (Eq. 15)$$

Where $H_R(T_A)$ is the enthalpy (J) of the reagents at a certain temperature (K), $H_P(T_A)$ is the enthalpy (J) of the products at a certain temperature (K) and m_f is the mass of fuel injected (g).

Thus, the higher the temperature, the higher the Net CHR and then, the higher the η_c. In this study, the reason for defining η_c is to estimate how complete the combustion is, which is related to the CHR. In this sense, under lean λ conditions, the amounts of incomplete products are small because there is enough O_2 to complete the combustion. On the other hand, under fuel-rich conditions, the amounts of incomplete combustion products increase, so a bigger fraction of the fuel CHR is not released, giving a higher Net CHR due to the lower $H_P(T_A)$. For this reason, the higher the λ, the lower the CHR.

Finally, according to Table 3.1 the higher the engine speed (N), the higher the VE (η_e), despite the expression shown in eq. 16.

$$\eta_e = \frac{2 \cdot \dot{m}_e}{\rho_{a,i} \cdot V_d \cdot N} = \frac{m_a}{\rho_{a,i} \cdot V_d} \qquad (Eq.16)$$

Where $\rho_{a,i}$ is the air density at atmospheric conditions (g/cm^3), $\dot{m}_e$ is the mass flow rate of fresh air intake (g/h) and m_a is the actual mass of air entering (g).

In this equation, the η_e is inversely proportional to the engine speed; nevertheless, the η_e is not reduced because the $\dot{m}_e$ also depends on the engine speed. In addition, V_d is fixed in the engine and $\rho_{a,i}$ is almost constant, so it only depends on the m_a. Therefore, at higher engine speed, more air enters because a higher vacuum is created in the cylinder, increasing η_e. .

On the other hand, in what respects to the λ, the higher the ratio, the lower the Power, Torque, BMEP, CHR and sNOx, because of the reduction of the temperatures reached during the combustion. On the other hand, the BTE, the BSFC remains practically in the same value, and the VE increases, due to the higher amount of air in the air-fuel mixture.

3.2. Fuels Comparison: Hydrogen, Methane and Coke oven gas.

This section intended to compare, the results obtained in different alternative fuels, such as CH_4 and COG, with the results obtained for the H_2, at the same λ and engine speed conditions; 3000 rpm and λ=1.5. For this reason, Figures 3.4, 3.5 and 3.6, are going to be explained below.

- Temperature (K) vs CA (◦):

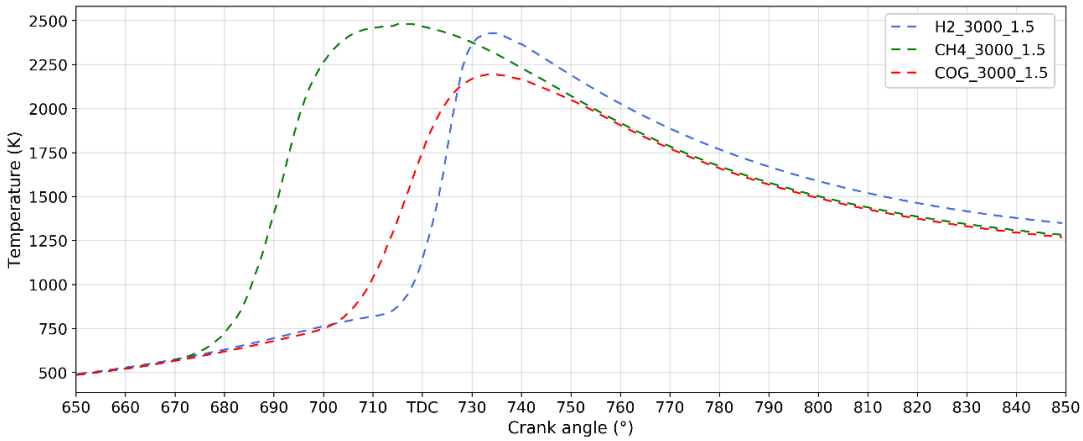

Figure 3.4. Temperature vs. CA for different fuels used at the same conditions.

The temperature behaviour, related to the CA and the SA, is the same in all the cases, but some differences can be appreciated besides their trend. First, the CH_4 starts the ignition so much earlier than the other fuels, the SA is higher than in the other cases, because the CH_4 owns the lowest reactivity, with the lowest S_L and the highest densities, so it requires the lowest PW and it is enhanced when the λ is reduced, in other words, when the mixture is enriched. For this reason, the CH_4 requires more time than the pure H_2 and COG. In the case of the last one, it needs more SA than H_2 because its mixture contains a big percentage of CH_4, but it also contains a high percentage of H_2, so it reacts faster than the pure CH_4, requiring an intermediate SA. Therefore, using a higher SA, the temperature reaches the highest value, and the maximum temperature stays longer in the cylinder because the piston still going up to the TDC, compressing the combustion products further, and hence, resulting in a longer combustion duration. In this sense, the BTE should become lower with pure CH_4, resulting in a higher BSFC of this fuel.

In addition, the COG reaches the lowest temperatures in the cylinder and the H_2 temperatures, after the TDC, remains slightly higher in the combustion chamber compared to the other fuels.

- Pressure (bar) vs CA (◦):

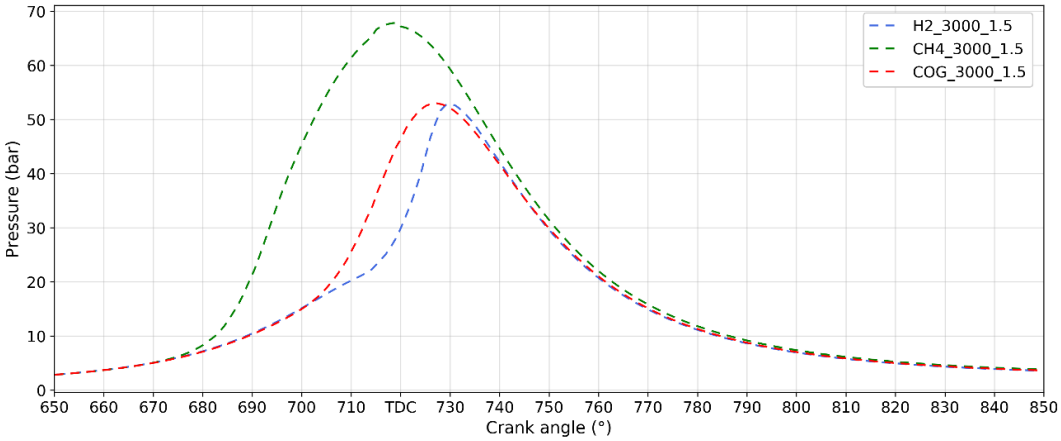

Figure 3.5. Pressure vs. CA for different fuels used at the same conditions.

In the case of the pressure behaviour, the CH_4 also owns the highest peak of pressure, and its duration is bigger as well, in the same way as with the temperature. In that way, the main difference compared to the temperature profiles, is the similar pressure reached in the COG and H_2, differing widely in the SA, but not that much in the pressure profile depicted. Then, as the most reactive fuel is H_2, it provides the shortest range of CA of increasing pressures during the combustion, due to the lowest SA.

However, despite the fact that usually the higher the pressure, the higher the power, the CH_4 should not obtain the highest engine performance, because in this case the pressure peak is reached before TDC, so after that the piston keeps rising and hence, it has to do a negative work to keep compressing those combustion gases. For this reason, the useful work is reduced, and the power output is lower.

- NO emissions (ppm) vs CA (◦):

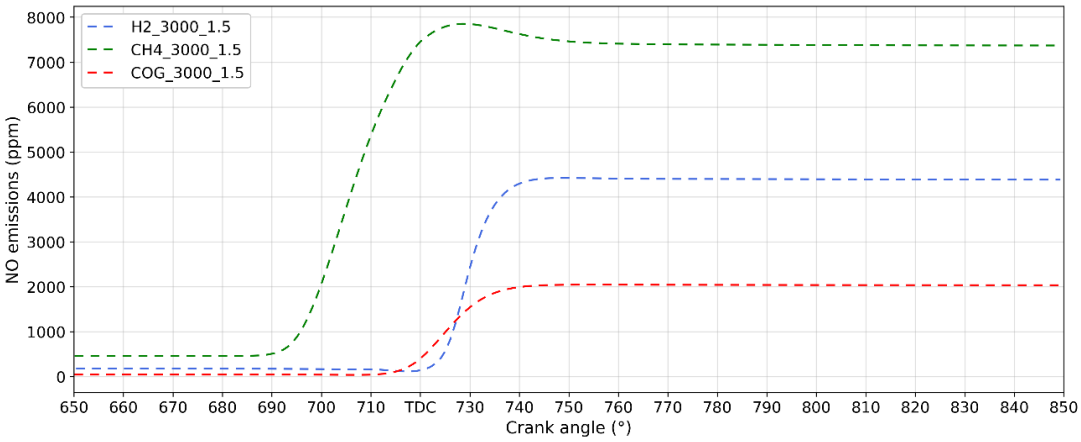

Figure 3.6. NO emissions vs. CA for different fuels used at the same conditions.

Theoretically, the H_2 has a stronger tendency to form NOx, because it used to get high combustion temperatures, but shorter combustion durations, promoting the formation of thermic NOx. In contrast to the CH_4, that should reduce the amount of NOx while reduce the combustion temperature reached. However, according to this figure the CH_4 generates the highest amount of NO emissions because it owns higher density and lower S_L, so the required SA is higher.

For this reason, in the case of the pure CH_4, the higher SA employed, explains the higher NOx formation, meanwhile the reduction in the NOx formation by using CH_4, is reflected in the case of COG that reaches a lower combustion temperature, reducing the NOx emissions, that are not so affected by the SA, in comparison with the CH_4, because it is closer to the SA used for the H_2 simulation. However, as can be seen in this figure, the levels of NOx are not so high neither in the case of pure H_2, and hence, through a blend with CH_4 and optimizing the SA, the NOx formation can be reduced even more in the H_2-ICE, without compromise the engine performance in terms of mechanical and energetical efficiency.

Based on the results of temperature, pressure and NOx emissions obtained in these simulations, the main parameters related to the engine performance have been calculated and are shown in Table 3.1.

Table 3.2. Engine Performance and emissions results obtained in H_2, CH_4 and COG simulations

Cycle 4	Power (kW)	Torque (Nm)	BMEP (bar)	BTE (%)	BSFC (g/kWh)	EV (%)	CHR (J)	sNO (g/kWh)
H_2: 3000 rpm λ=1.5	5.27	16.77	6.07	35.65	84.15	64.14	582.05	23.91
CH_4: 3000 rpm λ=1.5	3.92	12.46	4.51	26.90	267.70	76.76	575.45	60.73
COG: 3000 rpm λ=1.5	5.27	16.79	6.07	36.29	248.90	71.62	577.47	11.95

From this table, several conclusions can be extracted. At first, H_2 and COG have practically the same results regarding the Power, Torque, BMEP and BTE, in this sense, the performance of the engine obtained in terms of power and efficiency, is the same for both. On the other hand, although the CH_4 reaches the higest pressure, it has by far the lowest values in terms of engine performance. Therefore, has been demonstrated

that the effect of the SA in the pressure does not lead to an increase in the engine performance, because the lower reactivity of this component forces the engine to generate a negative work, resuting in power losses.

In the case of the H_2, it is the fuel with the lowest BSFC, therefore, is the most suitable fuel of the three in terms of needing less fuel to achieve the same performance as COG and more than CH_4. However, the COG has been obtained from the valorisation of a residual stream, so it is "free". Subsequently, in what respects to the VE, since H_2 is the lightest compound, its VE is the lowest, being the CH_4 the component with the highest VE, because it is the heaviest gas. In contrast, the CHR is very similar between the three gases, being the H_2 slightly higher than the others, and all of them have obtained high CHR values, which means that all have a very complete combustion reaction, enhancing the η_c.

Finally, the results of sNOx are very different depending on the fuel. At first, the CH_4 according to the higher combustion temperature reached and the longer duration, it produces the highest amount of NOx. However, in the COG can be found the reducing effect of CH_4 in the NOx formation, which produces the lowest amount of sNOx. Therefore, has been demonstrated that the effect of the SA in the temperature leads to an increase in the NOx emissions, and hence, the pure H_2 produces more thermic NOx than COG but lower than the CH_4.

4. Conclusions and Future Work

The main objective of this work is based on the development of simulations of a H_2-ICE at different operating conditions, studying their properties, analysing the weaknesses and strengths of the H_2 as fuel. Then, regarding the extensive methodology to apply and the deep description and selection of the main variables that help to describe the performance of the engine, the main conclusions were drawn from the study:

- Higher engine speed (rpm) increases the Power, due to the increase of the pressure, but also the sNOx emissions, due to the increase in the combustion temperature.

- Increasing the λ ratio employed, the engine performance is reduced in terms of Power, Torque, BMEP and CHR, because the mixture becomes leaner. However, reduces the emissions of NOx, due to the reduction of the combustion temperature.
- The SA exerts a strong influence on the levels of NOx emissions, increasing the combustion duration and the peaks of temperature. In that way, the higher the SA, the higher the amount of NOx generated. However, the increase in pressure with the increase of the SA, does not lead to an increase in engine performance.
- The H_2 and COG are the two main options of the three fuels, the pure CH_4 is the worst alternative in comparison with them, but can be used for enhancing the H_2 properties.
- The COG shows quite good properties in what respects to the engine performance and especially, the low emissions of NOx generated, turn it into a highly valuable alternative.
- Should be considered, that the COG is obtained as a residual stream from industrial processes, so it is "free" compared with the H_2 and CH_4 because it has not directly associated production costs.
- On the other hand, H_2 is the fuel with less BSFC so it means savings in the amount of fuel required to run the engine and provide the same engine performance as COG and higher engine performance than CH_4.

Finally, as future work, could be studied the influence of the engine speed and the lambda factor for the case of CH_4 and COG. In addition, other injection strategies, such as direct injection, compression ignition or the use of boosting systems such as superchargers and turbochargers could be studied, to improve the engine performance while reducing the emissions.

5. References

1. European Commission. The European Green Deal. Eur Comm [Internet]. 2019;53(9):24. Available from: https://eur-lex.europa.eu/legal-content/EN/TXT/PDF/?uri=CELEX:52019DC0640&from=EN

2. De Vita, A., Kielichowska, I., Mandatowa, P., Capros, P., Dimopoulou, E., Evangelopoulou, S., et al. Asset: Technology pathways in decarbonisation scenarios. 2018.

3. Andrei, M., Thollander, P., Pierre, I., Gindroz, B., and Rohdin, P. Decarbonization of the industry: Guidelines towards a harmonized energy efficiency policy program impact evaluation methodology. Energy Reports [Internet]. 2021;7:1385–95. Available from: https://doi.org/10.1016/j.egyr.2021.02.067

4. Vásquez, R. and Salinas, F. Tecnologías del hidrógeno y perspectivas para Chile. 2º Edition. Ministerio de Energía de Chile and Deutsche Gesellschaft für Internationale Zusammenarbeit (GIZ) GmbH. [Internet] 2019. Available from: Tecnologías-del-hidrógeno-y-perspectivas-para-Chile_2019.pdf (4echile-datastore.s3.eu-central-1.amazonaws.com)

5. ENEA: Consulting. The Potential of Power-To-Gas. [Internet] 2016;33(0):51. Available from: www.enea-consulting.com

6. Boretti, A. Hydrogen internal combustion engines to 2030. Int J Hydrogen Energy [Internet]. 2020;45(43):23692–703. Available from: https://doi.org/10.1016/j.ijhydene.2020.06.022

7. International Energy Agency. Technology Roadmap: Hydrogen and fuel cells. SpringerReference [Internet]. 2015;81. Available from: http://www.springerreference.com/index/doi/10.1007/SpringerReference_7300

8. IRENA. Green Hydrogen Cost Reduction: Scaling up Electrolysers to Meet the 1.50C Climate Goal [Internet]. 2020. 105 p. Available from: https://www.irena.org/-/media/Files/IRENA/Agency/Publication/2020/Dec/IRENA_Green_hydrogen_cost_2020.pdf

9. IRENA. Hydrogen From Renewable Power: Technology outlook for the energy transition [Internet]. 2018. 1–52 p. Available from: https://www.irena.org

10. Verhelst, B.S., Wallner, T., Eichlseder, H., and Naganuma, K. Electricity Powering Combustion: Hydrogen Engines. 2012;100(2).

11. Ortiz-Imedio, R., Ortiz, A., Urroz, I.C., Diéguez, P.M., Gorri, D., Gandía, L.M. and Ortiz, I. Comparative performance of coke oven gas, hydrogen and methane in a spark ignition engine. International Journal of Hydrogen Energy. 2021. Vol. 46, no. 33, p. 17572-17586. DOI: 10.1016/j.ijhydene.2019.12.165.

12. Aleiferis, Pavlos G. and Rosati, Martino F. Controlled autoignition of hydrogen in a direct-injection optical engine. Combustion and Flame. 2012. Vol. 159, no. 7, p. 2500-2515. DOI: 10.1016/j.combustflame.2012.02.021

13. Diéguez, P.M., Urroz, J.C., Sáinz, D., Machin, J., Arana, M., Gandía, L.M. Characterization of combustion anomalies in a hydrogen-fuelled 1.4 L commercial spark-ignition engine by means of in-cylinder pressure, block-engine vibration, and acoustic measurements. Energy Convers Manag [Internet]. 2018;172(July):67–80. Available from: https://doi.org/10.1016/j.enconman.2018.06.115

14. Fernández, C. Energética del hidrógeno. Contexto, estado actual y perspectivas de futuro. Tesis Dr Química Orgánica, Universidad de Sevilla, España [Internet]. 2013;73–81. Available from: www.unep.or.kr/energy/hydrogen/hyg_intro.htm

15. Heywood J.B. Internal combustion engine fundamentals. New York: McGraw-Hill Education; 1988.

16. Chincholkar S.P., Suryawanshi J.G. Gasoline Direct Injection: An Efficient Technology. Energy Procedia [Internet]. 2016; 90(December 2015):666–72. Available from: http://dx.doi.org/10.1016/j.egypro.2016.11.235

17. Verhelst S., Wallner T. Hydrogen-fuelled internal combustion engines. Prog Energy Combust Sci [Internet]. 2009;35(6):490–527. Available from: http://dx.doi.org/10.1016/j.pecs.2009.08.001

18. Reichel A., De Schoenmakere M., Gillabel J. Circular economy in Europe - developing the knowledge base (European Environment Agency Report No 2/2016) [Internet]. Publication Office of the European Union. 2016. 37 p. Available from: https://ec.europa.eu/environment/ecoap/policies-and-practices-eco-innovation-uptake-and-circular-economy-transition_en

19. Razzaq R., Li C., Zhang S. Coke oven gas: Availability, properties, purification, and utilization in China. Fuel [Internet]. 2013;113:287–99. Available from: http://dx.doi.org/10.1016/j.fuel.2013.05.070

20. Sopena C., Dieguez P.M., Sainz D., Urroz J.C., Guelbenzu E., Gandía L.M. Conversion of a commercial spark-ignition engine to run on hydrogen: performance comparison using hydrogen and gasoline. Int J Hydrogen Energy 2010; 35: 1420-9. DOI: https://doi.org/10.1016/j.ijhydene.2009.11.090.

21. Gregory P. Smith, David M. Golden, Michael Frenklach, Nigel W. Moriarty, Boris Eiteneer, Mikhail Goldenberg, C. Thomas Bowman, Ronald K. Hanson, Soonho Song, William C. Gardiner, Jr., Vitali V. Lissianski, and Zhiwei Qin. GRI-MECH Mechanism 3.0. [Internet]. University of Berkeley, California. Available from: http://www.me.berkeley.edu/gri_mech/

22. Liu, X., Liu, F., Zhou, L., Sun, B., and Schock, H. Backfire prediction in a manifold injection hydrogen internal combustion engine. International Journal of Hydrogen Energy. 2008. Vol. 33, no. 14, p. 3847-3855. DOI 10.1016/j.ijhydene.2008.04.051

6. Nomenclature

$\boldsymbol{A}$	Symmetric Injector Area
AEM	Anion Exchange Membrane
ALK	Alkaline Electrolysers
BDC	Bottom Dead Centre
BMEP	Brake Mean Effective Pressure
BSFC	Brake Specific Fuel Consumption
BTE or η_f	Brake Thermal Efficiency or fuel conversion efficiency
CA	Crank Angle
CAD	Computer-Aided Design
CFD	Computational Fluid Dynamics
CHR	Chemical Heat Release
CI	Compression-Ignition
COG	Coke Oven Gas
CR	Compression Ratio
dBTDC	degrees Before Top Dead Centre
EOI	End of Injection
EU	European Union
FCEVs	Fuel Cell Electric Vehicles
FCs	Fuel Cells
H_2-ICE	Hydrogen fuelled Internal Combustion Engine
HTS	High-Temperature Stage
$\boldsymbol{H_R(T_A)}$	Enthalpy of the reagents at a certain temperature
$\boldsymbol{H_P(T_A)}$	Enthalpy of the products at a certain temperature
ICEs	Internal Combustion Engines
Q_{HV}	Volumetric Lower Heating Value
LHV	Lower Heating Value
LTS	Low-Temperature Stage
MBT	Maximum Break Torque
MOFCs	Molten Carbonate Fuel Cells
MW	Molecular Weight
$\boldsymbol{m_{full}}$	Total mass of fuel injected
$\boldsymbol{\dot{m}_{NOx}}$	Mass flow of NOx produced during the combustion
$\boldsymbol{m(mg)}$	Exact fuel mass injected in milligrams
$\boldsymbol{\dot{m}_f}$	Mass flow of fuel injected
$\boldsymbol{\dot{m}_e}$	Mass flow of fresh air intake

m_a	Actual mass of air entering
m_{O_2}	Mass of Oxygen entered
N	Engine speed: Revolutions per second
NOx	Nitrogen Oxides
P	Power
PAFCs	Phosphoric Acid Fuel Cells
PEM	Proton Exchange Membrane Electrolysers
PEMFCs	Proton Exchange Membrane Fuel Cells
PFI	Port Fuel Injection
PSA	Pressure Swing Adsorption
PW	Pulse Width
RPM	Engine speed: Revolutions Per Minute
SA	Spark Advance
SI	Spark-Ignition
SL	Laminar Flame Speed
SMR	Steam Methane Reforming
sNOx	Specific Nitrogen Oxide emissions
SOEC	Solid Oxide Electrolyser
SOFCs	Solid Oxide Fuel Cells
T	Torque
TDC	Top Dead Centre
TKE	Turbulent Kinetic Energy
VE or η_e	Volumetric efficiency
V_d	Cylinder volume displaced by the piston in all the cylinders
v_i	Injection velocity of each fuel
WOT	Wide Open Throttle
$W_{c,i}$	Work delivered per cycle
λ	Lambda factor: Air-Fuel Ratio
λ_{st}	Stoichiometric Air-Fuel Ratio
λ_{Rel}	Relative Air-Fuel Ratio
λ_{Actual}	Actual Air-Fuel Ratio
η_R	Number of crank revolutions for each power stroke per cylinder
η_c	Combustion efficiency
ρ_i	Injection density of each fuel
$\rho_{a,i}$	Air density at atmospheric conditions
Φ	Equivalence Ratio

7. Annexes

Annex A. ANSYS Basics.

Annex A. I. How to import in ANSYS.

First, inside of the ANSYS Workbench, on the left window, called “Toolbox”, there is a list of tools that can be used, so to import the existent geometry is required to click in the “Component Systems” tab, then in the “Geometry” icon of this list and drag it to the “Project Schematic” which is the big white window, and the standalone system is already created. Afterwards, making a right-click on the system “A”, appeared on the screen like an array, the option “New SpaceClaim Geometry” has to be opened as can be seen in Figure A.1.

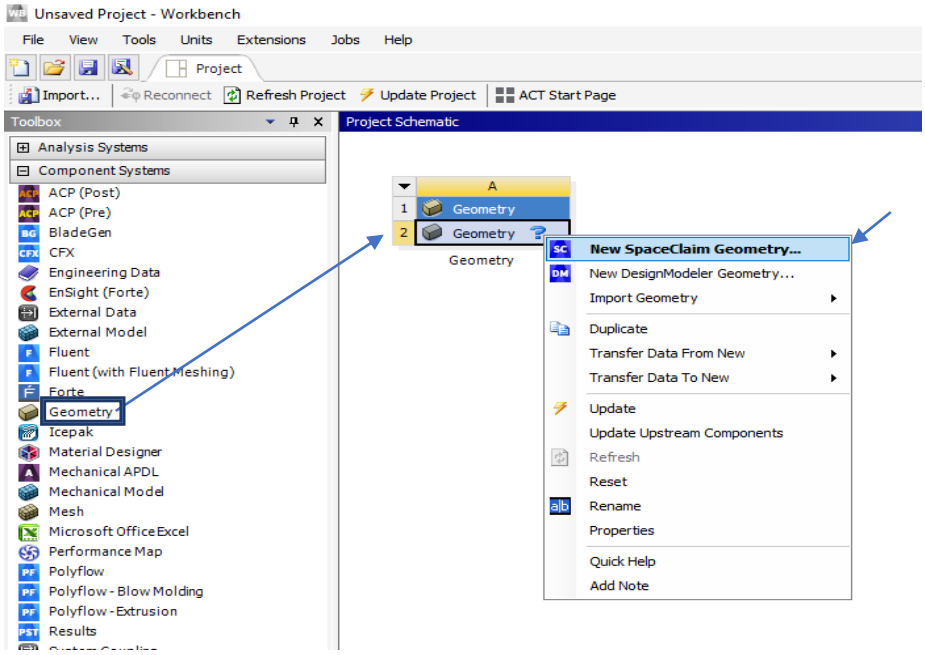

Figure A.1. How to import a geometry in ANSYS Workbench, using SpaceClaim.

Once the SpaceClaim is opened, the Inventor file must be imported. However, when a file is imported in SpaceClaim from other CAD software, this tool separates all the surfaces previously created, for instance, on Inventor, turning each object into some different pieces contained in one solid geometry. Then, it is required to join all these pieces, defining each face of the engine. For this reason, it is important to know which are the pieces that compose each part of the designed engine, being careful of the symmetry is parallel to the “Z” axis. The design is shown in Figure A.2.

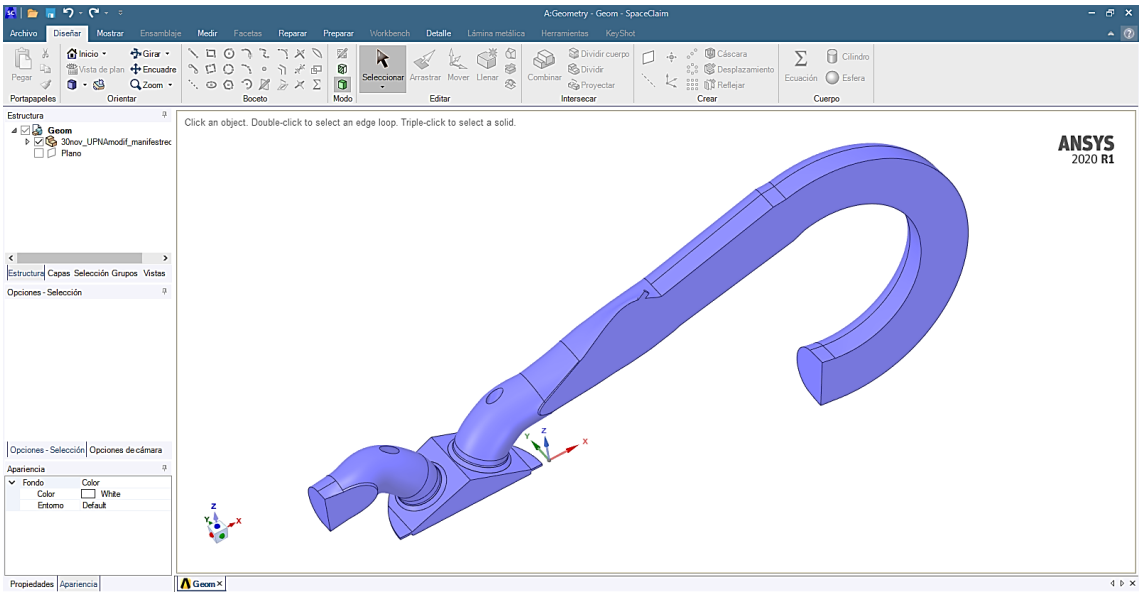

Figure A.2. Geometry Model imported in SpaceClaim.

To do this is needed to go back to the ANSYS Workbench and drag the “Mesh” icon from the Toolbox to the right side of the SpaceClaim system “A” and afterwards the “A2” raw of the geometry system is transferred to the “B2” of the Mesh system “B”, now the geometric design has been already imported to the Mesh tool. Finally, in the same way, that SpaceClaim, the Mesh is opened, as can be seen in Figure A.3.

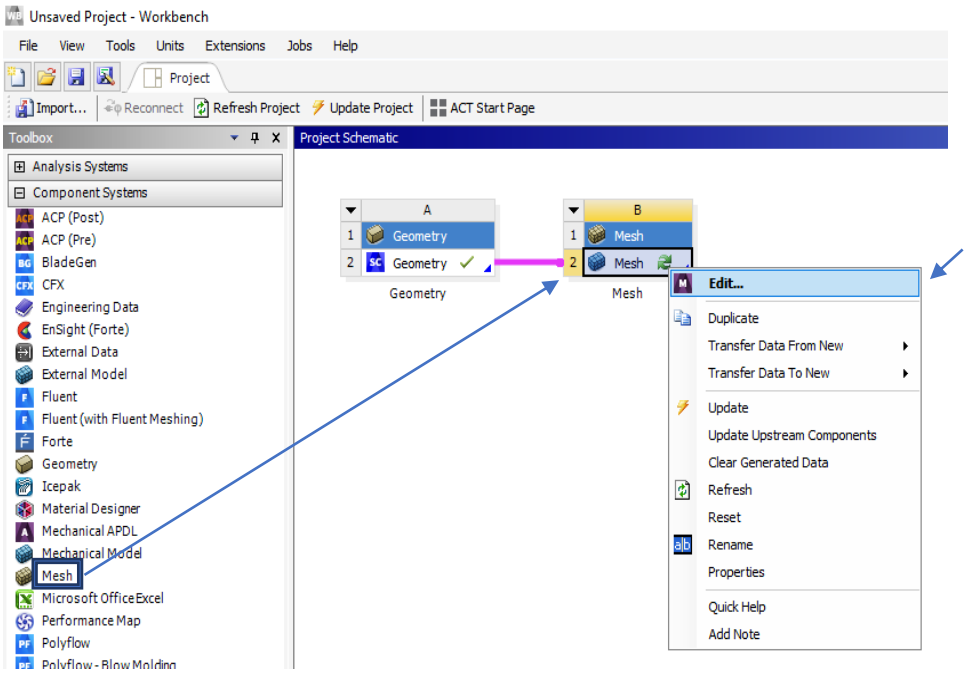

Figure A.3. How to import geometry from SpaceClaim to Mesh in the ANSYS Workbench.

ANSYS Forte is the CFD code software in charge to carry out the simulation. Therefore, in the same way, that was imported the geometry into the Mesh, now, the Mesh must be imported into ANSYS Forte in the ANSYS Workbench project schematic window, resulting in the flowsheet of the project that appears in Figure A.4.

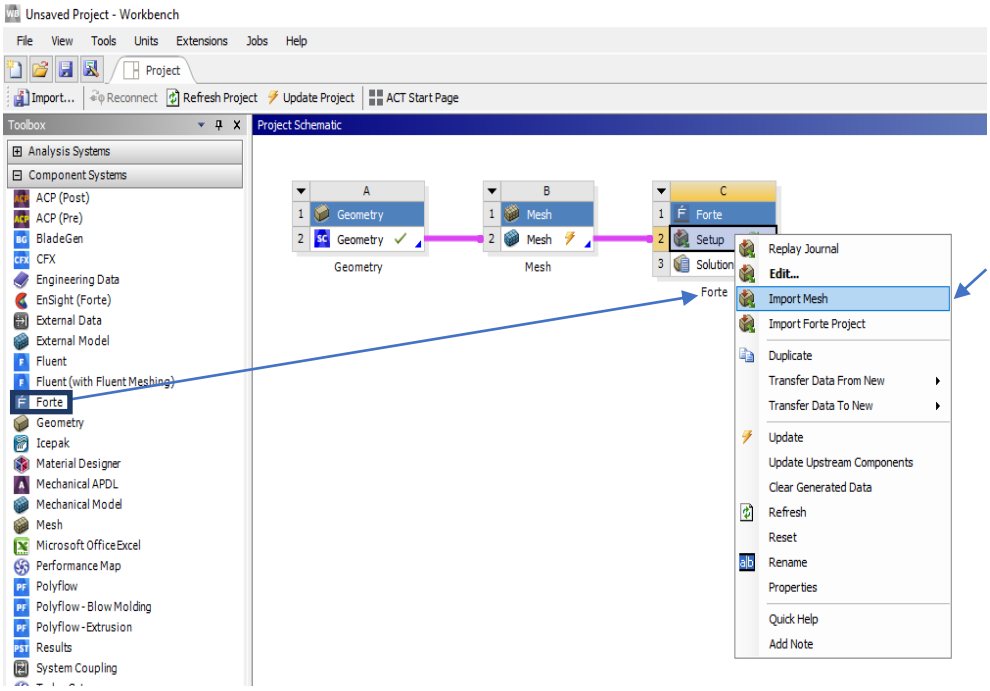

Figure A.4. How to import the meshing to ANSYS Forte in the ANSYS Workbench.

In this case, the Mesh row, which is the B2, is joined to the C2 raw called “Set up” and to go inside Forte is clicked the right button and “Update” is selected. Once Forte is opened, different windows can be seen on the screen, as is shown in Figure A.5.

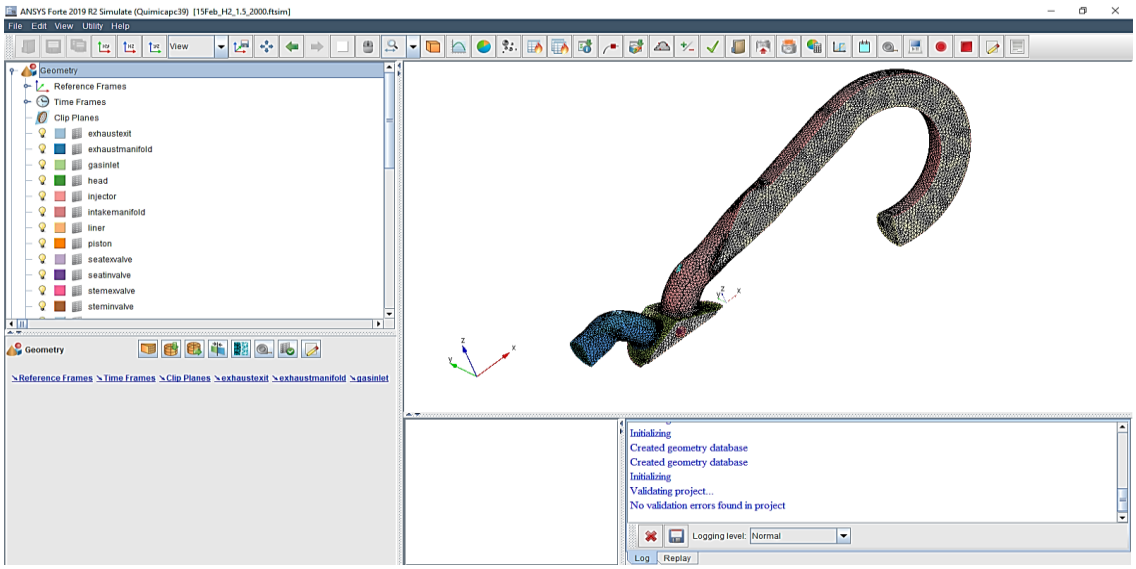

Figure A.5. ANSYS Forte simulation software.

Annex A. II. How to make a suitable Mesh.

Once the Mesh is opened, it is necessary to define the corresponding surfaces that belong to each part of the engine. First, to select the related surfaces, it is necessary to click on the "Face" select mode, and then, click on the different surfaces, when all the surfaces of one part, for instance, the piston, are selected, with the right button click, and clicking in "Create named selection", the last thing is to write the name of the object, in this case, "piston" and do it with the rest of the parts that are going to appear in the "Named selections" outline on the left window, up to get the named selections that appear hereunder in Figure A.6.

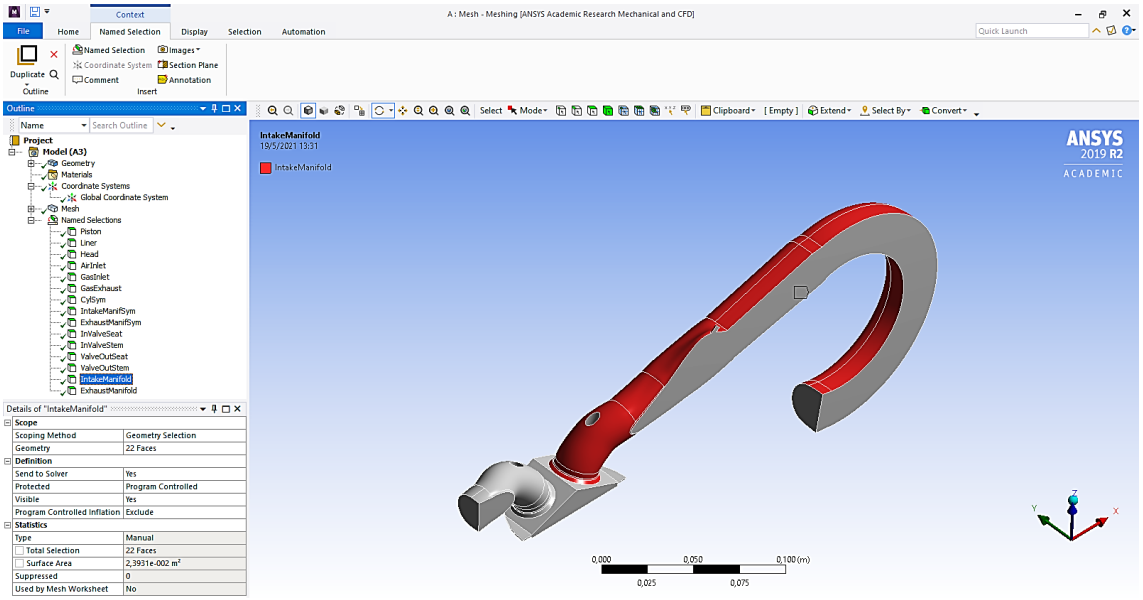

Figure A.6. Creating Named Selections in Mesh, before the meshing.

It is important to note that some surfaces are hidden behind others that are not used in the required surface, as occurs with the valves, so in those cases, it is needed to be very accurate, starting from the external parts and finishing with the internal constituents. With all the parts well defined, it is time to create the geometric mesh, first, clicking in "Mesh" outline inside of the left window, and applying the data for the global meshing, selecting "Hydrodynamics" as "Physics Reference" and defining the overall element size of the mesh. The element size is referred to the size of each cell of the mesh, therefore, the bigger the element size, the less accurate the geometric meshing and afterwards the simulation results are further away from the desired, conversely, the smaller the element size, the more suitable will be the geometrical

mesh to obtain more realistic results in the simulation step and hereinafter when a mesh value is applied it is highly recommended to click on “Update” to save the changes and work properly. Finally, the most important step is the generation of more refined meshes in the key sections of the engine geometry. In that way, for the “Scoping method” in which the desired to be refined faces are going to be defined, it is possible to choose among two options; “Named selections” or “Geometry Selection”, depending on if it is required the entire component or just only some faces of this component of the engine. In this sense, just only the seat of both valves; “ValveInSeat” and the “ValveOutSeat” are scoped as named selections because these parts must fit into the notches of the piston and their respective manifolds. On the other hand, the geometry selection faces belong to:

- Injector: Refining the cross-section and injector wall, keeping the overall element size for the internal face which is cut-off by the symmetry. The shape of the injector section has a strong influence on how works fuel injection.

- Piston: Refining the notches and the junction on the bottom surface of the piston, because they must fit with the valves to avoid design problems limiting engine performance.

- Manifolds: Refining the intake and exhaust junction between the head of the cylinder and the manifolds, to fit this joint with the shape of the seat valves.

- Symmetry: Refining the junctions between the manifolds and the cut-of symmetry faces and to keep the details of these junctions “Capture Curvature” is also activated with the default values.

Applying these values and following all these steps, the data of the mesh is represented below in Figure A.7.

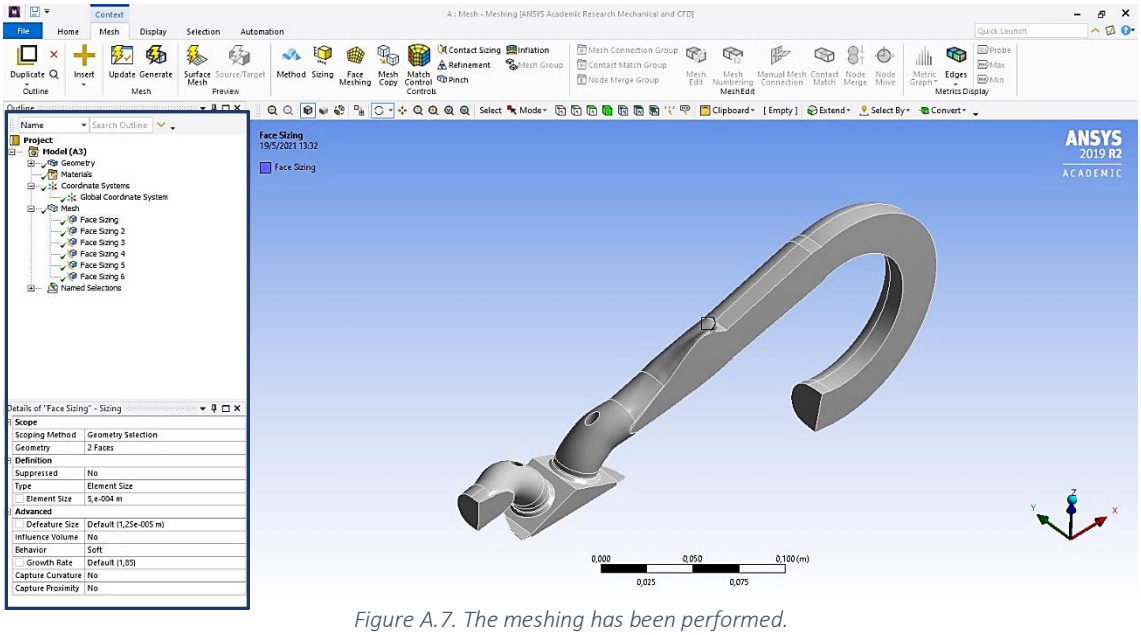

Figure A.7. The meshing has been performed.

Annex A. III. How to see the results and develop an iterative process.

The figure shows the two most important windows are the window on the right side which shows the engine modelled with the geometric meshing previously applied and on the left side the workflow tree. The last one includes some functions and specifications where are going to be included in all the parameters and variables to run the simulation as can be seen in Figure A.8.

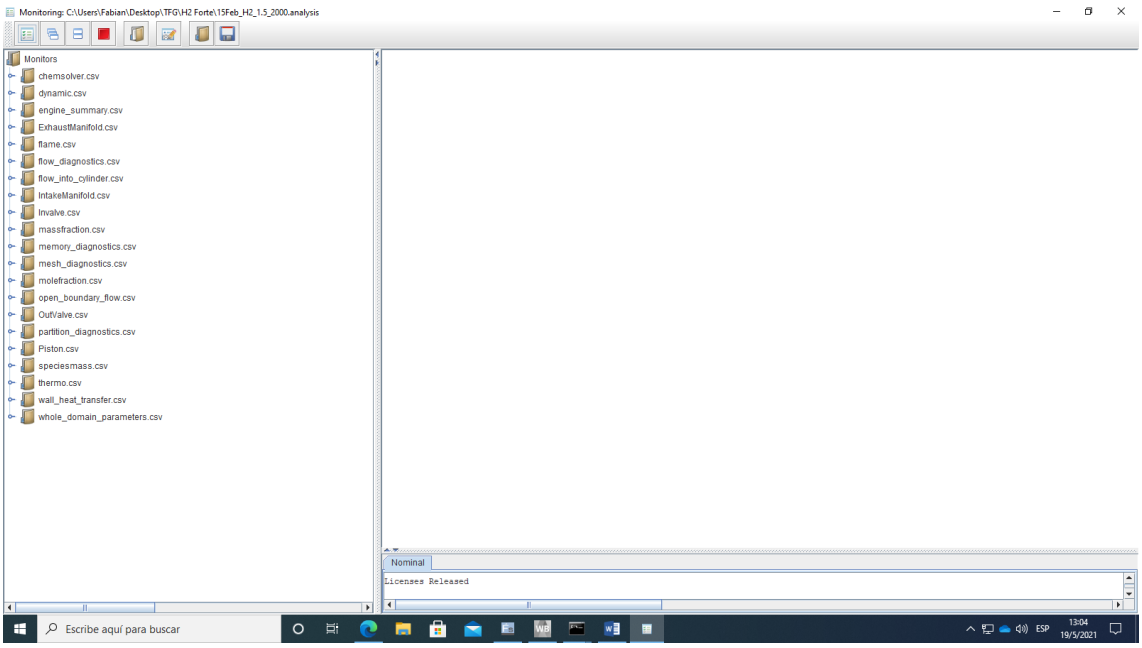

Figure A.8. ANSYS Forte Monitoring Results after the simulation has finished.

In the monitor, there are some important parameters to carry out the next simulations with more accuracy such as; the Temperature, the pressure and the Turbulent Kinetic Energy (TKE) in the “Thermo.csv” file and the same file the “In-Cylinder averaged equivalence ratio” that represents the inverse of λ, well-known as ϕ, that gives the required information to determine how good has been performed the simulation, as can be seen in Figure A.9.

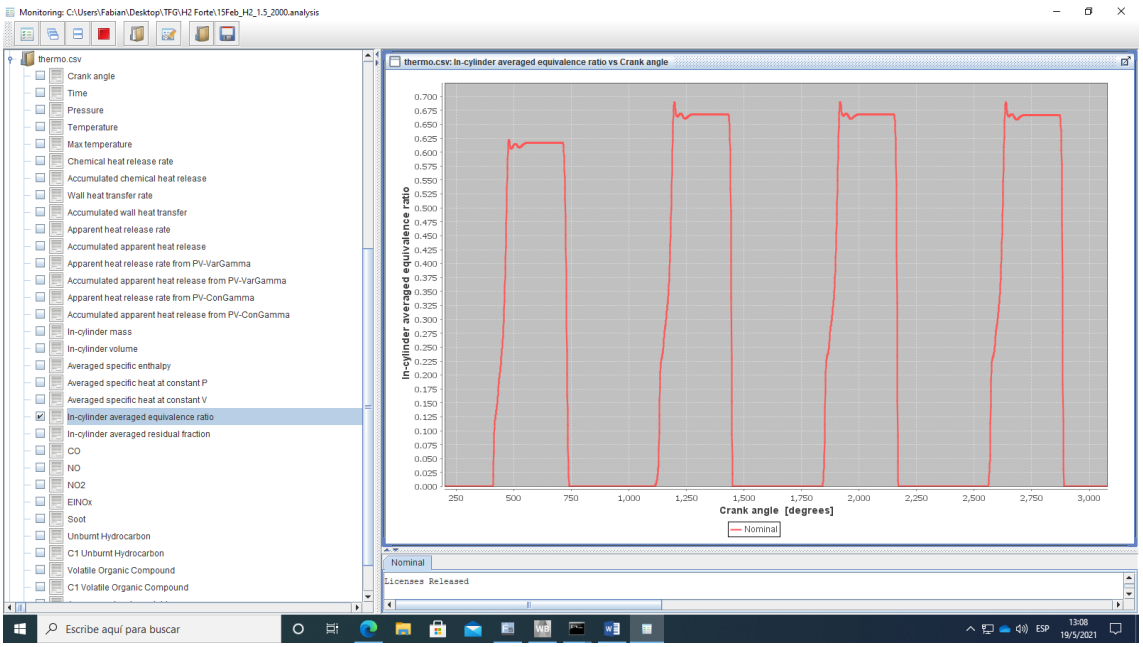

Figure A.9. In-Cylinder averaged equivalence ratio.

Therefore, whether the ratio is far from the desired value, this simulation has to be repeated up to reach the closer value possible to the λ fixed for the simulation.

In addition, it is important to highlight that the results are measured at the end of the simulation, at 3080 ^{o}, because the fourth cycle is the more representative due to these results are stabilised and represents better the real results than in the first cycle.

Annex B. Calculations.

Annex B. I. Air Fuel Ratio (λ).

The calculations are going to be performed for every fuel (Hydrogen, Methane and Coke Oven Gas):

Hydrogen (H_2).

First, look at the stoichiometry of the reaction:

$$H_2 + \frac{1}{2} O_2 \rightarrow H_2O$$

Then, the mass flow of the reagents of interest must be calculated at STP conditions. Beginning with the calculation of the total molar flow (σ_{H_2}):

- Based on the Ideal Gas Law:

$$P \cdot V = n \cdot R \cdot T$$

$$n_{H_2} = \sigma_{H_2} = \frac{P \cdot V}{R \cdot T}$$

- According to the STP conditions and making one assumption for the volumetric flow (Q_{H_2}):

$$P = 1\ atm$$

$$T = 273.15\ K$$

$$R = 0.082\ \left(\frac{atm \cdot L}{mol \cdot K}\right)$$

$$Q_{H_2} = 100\ \left(\frac{NL}{min}\right) \rightarrow Assumption$$

- Substituting in the Ideal Gas Law:

$$\sigma_{H_2} = \mathbf{4.462}\ \left(\frac{\boldsymbol{mol}}{\boldsymbol{min}}\right) = \boldsymbol{\sigma_{Fuel}}$$

The H_2 molar flow is the molar flow of the fuel because its molar fraction is equal to 1 (Pure H_2). Therefore, knowing its Molecular Weight (MW):

$$\dot{m}_{H_2} = \sigma_{H_2} \cdot MW_{H_2} = 4.462\ \frac{mol\ H_2}{min} \cdot \frac{1\ min}{60\ s} \cdot \frac{2.016\ g\ H_2}{1\ mol\ H_2} = \mathbf{0.150} \left(\frac{\boldsymbol{g\ H_2}}{\boldsymbol{s}}\right) = \boldsymbol{\dot{m}_{fuel}}$$

This is the mass flow of fuel, so only the mass flow of air, calculated based on the mass flow of oxygen (O_2), is missing. Therefore, the molar flow of O_2 must be calculated:

$$\sigma_{O_2} = v_{O_2} \cdot \sigma_{H_2} = \left(\frac{1\ mol\ O_2}{2\ mol\ H_2}\right) \cdot 4.462\ \left(\frac{mol\ H_2}{min}\right) = \mathbf{2.231}\ \left(\frac{\boldsymbol{mol\ O_2}}{\boldsymbol{min}}\right)$$

In the air the composition is 21% O_2 and 79% Nitrogen (N_2), so applying the rule of three, the molar flow of air is calculated:

$$\sigma_{Air} = 2.231\left(\frac{mol\ O_2}{min}\right)\cdot\frac{100}{21}\cdot\frac{1\ min}{60\ s} = \mathbf{0.177}\left(\frac{\boldsymbol{mol\ Air}}{\boldsymbol{s}}\right)$$

Then, knowing its MW:

$$\dot{m}_{Air} = \sigma_{Air}\cdot MW_{Air} = 0.177\ \frac{mol\ air}{s}\cdot\frac{28.966\ g\ Air}{1\ mol\ Air} = \mathbf{5.128}\left(\frac{\boldsymbol{g\ Air}}{\boldsymbol{s}}\right)$$

Afterwards, the stoichiometric lambda (λ_{st}) is calculated:

$$\lambda_{St} = \frac{\dot{m}_{Air}}{\dot{m}_{fuel}} = \frac{5.128\ \frac{g\ Air}{s}}{0.150\ \frac{g\ H_2}{s}} \approx \mathbf{34.212}\ \left(\frac{\boldsymbol{g\ Air}}{\boldsymbol{g\ H_2}}\right)$$

Finally, from the desired relative Lambda (λ_{Rel}), the amount of mass of air or fuel that is held in the simulation, can be calculated:

$$\lambda_{Rel} = \frac{\lambda_{Actual}}{\lambda_{St}} \rightarrow 1.5 = \frac{\left(\frac{\dot{m}_{Air}}{\dot{m}_{fuel}}\right)_{Actual}}{34.212}$$

Methane (CH_4).

The same procedure is followed as in the previous case. First, look at the stoichiometry of the reaction:

$$CH_4 + 2O_2 \rightarrow CO_2 + 2H_2O$$

Then, the mass flow of the reagents of interest must be calculated at STP conditions. Beginning with the calculation of the total molar flow (σ_{CH_4}):

$$\sigma_{CH_4} = \mathbf{4.462}\ \left(\frac{\boldsymbol{mol}}{\boldsymbol{min}}\right) = \boldsymbol{\sigma_{Fuel}}$$

The CH_4 molar flow is the molar flow of the fuel because its molar fraction is equal to 1 (Pure CH_4). Therefore, knowing its Molecular Weight (MW):

$$\dot{m}_{fuel} = \sigma_{CH_4} \cdot MW_{CH_4} = 4.462\ \frac{mol\ CH_4}{min} \cdot \frac{1\ min}{60\ s} \cdot \frac{16.043\ g\ CH_4}{1\ mol\ CH_4} = \mathbf{1.193}\left(\frac{\boldsymbol{g\ CH_4}}{\boldsymbol{s}}\right)$$

This is the mass flow of fuel, so only the mass flow of air, calculated based on the mass flow of oxygen (O_2), is missing. Therefore, the molar flow of O_2 must be calculated:

$$\sigma_{O_2} = v_{O_2} \cdot \sigma_{CH_4} = \left(\frac{2\ mol\ O_2}{1\ mol\ CH_4}\right) \cdot 4.462\ \left(\frac{mol\ CH_4}{min}\right) = \mathbf{8.923}\ \left(\frac{\boldsymbol{mol\ O_2}}{\boldsymbol{min}}\right)$$

In the air the composition is 21% O_2 and 79% Nitrogen (N_2), so applying the rule of three, the molar flow of air is calculated:

$$\sigma_{Air} = 8.923\left(\frac{mol\ O_2}{min}\right) \cdot \frac{100}{21} \cdot \frac{1\ min}{60\ s} = \mathbf{0.708}\left(\frac{\boldsymbol{mol\ Air}}{\boldsymbol{s}}\right)$$

Then, knowing its MW:

$$\dot{m}_{Air} = \sigma_{air} \cdot MW_{air} = 0.708\ \frac{mol\ air}{s} \cdot \frac{28.966\ g\ Air}{1\ mol\ Air} = \mathbf{20.513}\left(\frac{\boldsymbol{g\ Air}}{\boldsymbol{s}}\right)$$

Afterwards, the stoichiometric lambda (λ_{st}) is calculated:

$$\lambda_{St} = \frac{\dot{m}_{Air}}{\dot{m}_{fuel}} = \frac{20.513\ \frac{g\ Air}{s}}{1.193\ \frac{g\ CH_4}{s}} \approx \mathbf{17.196}\ \left(\frac{\boldsymbol{g\ Air}}{\boldsymbol{g\ CH_4}}\right)$$

Finally, from the desired relative Lambda (λ_{Rel}), the amount of mass of air or fuel that is held in the simulation, can be calculated:

$$\lambda_{Rel} = \frac{\lambda_{Actual}}{\lambda_{St}} \rightarrow 1.5 = \frac{\left(\frac{\dot{m}_{air}}{\dot{m}_{fuel}}\right)_{Actual}}{17.196}$$

Coke Oven Gas (COG).

In this case, the procedure is a little bit complex. First, look at the stoichiometry of the reaction:

$$H_2 + \frac{1}{2}O_2 \rightarrow H_2O$$

$$CH_4 + 2O_2 \rightarrow CO_2 + 2H_2O$$

$$CO + \frac{1}{2} O_2 \rightarrow CO_2$$

In contrast to the pure H_2 and CH_4 calculations, in this case, the species and their compositions, in terms of volumetric fraction, given by Table 1.2, must be considered. Therefore, knowing the total molar flow of fuel at STP conditions:

$$\sigma_{fuel} = \mathbf{4.462} \left(\frac{\boldsymbol{mol}}{\boldsymbol{min}}\right)$$

The molar flows of each species can be calculated:

$$\sigma_{H_2} = 0.57 \cdot 4.462 \left(\frac{mol}{min}\right) = \mathbf{2.543} \left(\frac{\boldsymbol{mol\ H_2}}{\boldsymbol{min}}\right)$$

$$\sigma_{CH_4} = 0.30 \cdot 4.462 \left(\frac{mol}{min}\right) = \mathbf{1.339} \left(\frac{\boldsymbol{mol\ CH_4}}{\boldsymbol{min}}\right)$$

$$\sigma_{CO} = 0.06 \cdot 4.462 \left(\frac{mol}{min}\right) = \mathbf{0.268} \left(\frac{\boldsymbol{mol\ CO}}{\boldsymbol{min}}\right)$$

$$\sigma_{CO_2} = 0.02 \cdot 4.462 \left(\frac{mol}{min}\right) = \mathbf{0.089} \left(\frac{\boldsymbol{mol\ CO_2}}{\boldsymbol{min}}\right)$$

$$\sigma_{N_2} = 0.05 \cdot 4.462 \left(\frac{mol}{min}\right) = \mathbf{0.223} \left(\frac{\boldsymbol{mol\ N_2}}{\boldsymbol{min}}\right)$$

Then, every mass flow can be calculated knowing the MW of each species, and the sum of all of them gives back the mass flow of the fuel (COG):

$$\dot{m}_{COG} = \sum_{i=H_2}^{n} (\sigma_i \cdot MW_i) \cdot \frac{1\ min}{60\ s} = \mathbf{0.738} \left(\frac{\boldsymbol{g\ COG}}{\boldsymbol{s}}\right) = \boldsymbol{\dot{m}_{fuel}}$$

In addition, the MW_{COG} can be calculated as the sum of all the MW of these species multiplied by their composition in the fuel (%vol):

$$MW_{COG} = \sum_{i=H_2}^{n} \left(\frac{\%vol_i}{100} \cdot MW_i\right) = \mathbf{9.923} \left(\frac{\boldsymbol{g\ COG}}{\boldsymbol{mol}}\right)$$

In the case of the O_2, as it appears in the three main combustion reactions, its molar flow is calculated as the sum of the three, using the reaction stoichiometry:

$$\sigma_{O_2} = \frac{1}{2} \cdot \sigma_{H_2} + \mathbf{2} \cdot \sigma_{CH_4} + \frac{1}{2} \cdot \sigma_{CO} = \mathbf{4.082} \left(\frac{\boldsymbol{mol\ O_2}}{\boldsymbol{min}}\right)$$

In the air the composition is 21% O_2 and 79% Nitrogen (N_2), so applying the rule of three, the molar flow of air is calculated:

$$\sigma_{Air} = 4.082 \left(\frac{mol\ O_2}{min}\right) \cdot \frac{100}{21} \cdot \frac{1\ min}{60\ s} = \mathbf{0.324} \left(\frac{\boldsymbol{mol\ Air}}{\boldsymbol{s}}\right)$$

Then, knowing its MW:

$$\dot{m}_{Air} = \sigma_{air} \cdot MW_{air} = 0.324\ \frac{mol\ Air}{s} \cdot \frac{28.966\ g\ Air}{1\ mol\ Air} = \mathbf{9.385} \left(\frac{\boldsymbol{g\ Air}}{\boldsymbol{s}}\right)$$

Afterwards, the stoichiometric lambda (λ_{st}) is calculated:

$$\lambda_{St} = \frac{\dot{m}_{Air}}{\dot{m}_{fuel}} = \frac{9.385\ \frac{g\ Air}{s}}{0.738\ \frac{g\ COG}{s}} \approx \mathbf{12.718} \left(\frac{\boldsymbol{g\ Air}}{\boldsymbol{g\ H_2}}\right)$$

Finally, from the desired relative Lambda (λ_{Rel}), the amount of mass of air or fuel that is held in the simulation, can be calculated:

$$\lambda_{Rel} = \frac{\lambda_{Actual}}{\lambda_{St}} \rightarrow 1.5 = \frac{\left(\frac{\dot{m}_{air}}{\dot{m}_{fuel}}\right)_{Actual}}{12.718}$$

Annex B. II. Injection velocity.

The injection velocity is calculated using the equation shown below:

$$v_i \left(\frac{m}{s}\right) = \frac{\dot{m}_i \left(\frac{g}{s}\right)}{\rho_i \left(\frac{g}{cm^3}\right) \cdot A(cm^2) \cdot 100 \left(\frac{cm}{m}\right)}$$

To obtain its value, that must be constant during all the width of the injection pulse or Pulse Width (PW), the density of the fuel during the pulse that enters through the injector (ρ), the injection area (A) or section, that has been cut off by the symmetry, and the mass flow of fuel injected, have to be known. In this sense, the A (cm^2) is given by the geometry design:

$$A_{Total\ Injector} = 0.089\ cm^2$$

However, the simulation is performed on the symmetric engine, hence, the injection area is:

$$A_{Symmetric\ injector} = A = \frac{0.089\ cm^2}{2} = \mathbf{0.0445\ cm^2}$$

Afterwards, the density of each fuel in the injector is calculated. To make this calculation, the density can be obtained through the Ideal Gases Law:

$$P \cdot V = n \cdot R \cdot T = \frac{m}{MW} \cdot R \cdot T$$

$$P \cdot MW = \frac{m}{V} \cdot R \cdot T = \rho \cdot R \cdot T$$

$$\rho = \frac{P \cdot MW_i}{R \cdot T}$$

Now, setting the operating conditions for the injection:

$$P = 3\ bar$$

To obtain a constant injection velocity, the pressure of the injection was fixed at the value.

$$MW_{H_2} = 2.016 \left(\frac{g\ H_2}{mol}\right)$$

$$MW_{CH_4} = 16.043 \left(\frac{g\ CH_4}{mol}\right)$$

$$MW_{COG} = 9{,}923 \left(\frac{g\ COG}{mol}\right)$$

Then, substituting in the Ideal Gases Law, the injection density is determined for each fuel:

$$\rho_{H_2} = \frac{3\ bar \cdot 2.01568 \left(\frac{g\ H_2}{mol}\right)}{0.08314 \left(\frac{bar \cdot L}{mol \cdot K}\right) \cdot \frac{1000\ cm^3}{1\ L} \cdot 298.15\ K} = \mathbf{0.000244} \left(\frac{\boldsymbol{g\ H_2}}{\boldsymbol{cm^3}}\right)$$

$$\rho_{CH_4} = \frac{3\ bar \cdot 16.043\ \left(\frac{g\ CH_4}{mol}\right)}{0.08314\ \left(\frac{bar \cdot L}{mol \cdot K}\right) \cdot \frac{1000\ cm^3}{1\ L} \cdot 298.15\ K} = \mathbf{0.001942}\left(\frac{\boldsymbol{g\ CH_4}}{\boldsymbol{cm^3}}\right)$$

$$\rho_{COG} = \frac{3\ bar \cdot 9.923\left(\frac{g\ COG}{mol}\right)}{0.08314\ \left(\frac{bar \cdot L}{mol \cdot K}\right) \cdot \frac{1000\ cm^3}{1\ L} \cdot 298.15\ K} = \mathbf{0.001201}\left(\frac{\boldsymbol{g\ COG}}{\boldsymbol{cm^3}}\right)$$

Finally, the mass flow value was assumed in each case, based on the Physico-chemical properties of each fuel and the previous experimental studies on this engine, as can be seen, summarized below in Table B.1.

Table B.1. Total, and Symmetry Total Mass Flow Rates for each gas during the injection.

Gas	Total Mass Flow Rate (g/s)	For the symmetry in Forte (g/s)
H_2	0.6	0.3
CH_4	2	1
COG	1.4	0.7

The symmetry values are the values used in these calculations, in the same way, that the symmetrical area is used. Therefore, the injection velocity can be determined for each case, as shown below:

$$v_{H_2}\left(\frac{m}{s}\right) = \frac{0.3\ \left(\frac{g}{s}\right)}{0.000244\ \left(\frac{g}{cm^3}\right) \cdot 0.0445(cm^2) \cdot 100\left(\frac{cm}{m}\right)} = \mathbf{275}\left(\frac{\boldsymbol{m}}{\boldsymbol{s}}\right)$$

$$v_{CH_4}\left(\frac{m}{s}\right) = \frac{1\ \left(\frac{g}{s}\right)}{0.001942\ \left(\frac{g}{cm^3}\right) \cdot 0.0445(cm^2) \cdot 100\left(\frac{cm}{m}\right)} = \mathbf{115}\left(\frac{\boldsymbol{m}}{\boldsymbol{s}}\right)$$

$$v_{COG}\left(\frac{m}{s}\right) = \frac{0.7\ \left(\frac{g}{s}\right)}{0.001201\ \left(\frac{g}{cm^3}\right) \cdot 0.0445(cm^2) \cdot 100\left(\frac{cm}{m}\right)} = \mathbf{130}\left(\frac{\boldsymbol{m}}{\boldsymbol{s}}\right)$$

Annex B. III. Pulse Width (PW).

The PW is calculated using the equation shown below:

$$PW = \frac{N\ \left(\frac{^\circ}{s}\right)}{\dot{m}\ \left(\frac{g}{s}\right)}$$

Where:

$N\ = Is\ the\ engine\ speed.$

$\dot{m}\ = Is\ the\ mass\ flow\ in\ the\ injection\ of\ each\ fuel.$

$m_{full} = Is\ the\ total\ amount\ of\ fuel\ injected\ after\ all\ the\ PW$

Then, the mass flows and the engine speed are known, but the amount of fuel injected in each case has to be calculated. In that way, this parameter can be obtained from the λ_{Rel} expression:

$$\lambda_{Rel} = \frac{\lambda_{Actual}}{\lambda_{St}} = \frac{\left(\frac{\dot{m}_{Air}}{\dot{m}_{fuel}}\right)_{Actual}}{\lambda_{St}} = \frac{\frac{100}{21}\cdot\sigma_{O_2}\cdot Mw_{Air}}{\frac{m_{fuel}}{\lambda_{St}}}$$

$$\lambda_{Rel} = \frac{\frac{100}{21}\cdot\frac{m_{O_2}}{MW_{O_2}}\cdot Mw_{Air}}{\frac{m_{fuel}}{\lambda_{St}}} \rightarrow\ m_{fuel} = \frac{\frac{100}{21}\cdot\frac{m_{O_2}}{MW_{O_2}}\cdot Mw_{Air}}{\lambda_{Rel}\cdot\lambda_{St}}$$

Finally, assuming the mass of O_2 added for each case, based on the Physico-chemical properties of each fuel and iterating based on the values obtained in each simulation, the PW for every simulation is calculated.

Annex C. Profile imported in ANSYS Forte.

Annex C. I. Pulse Width (PW) profiles.

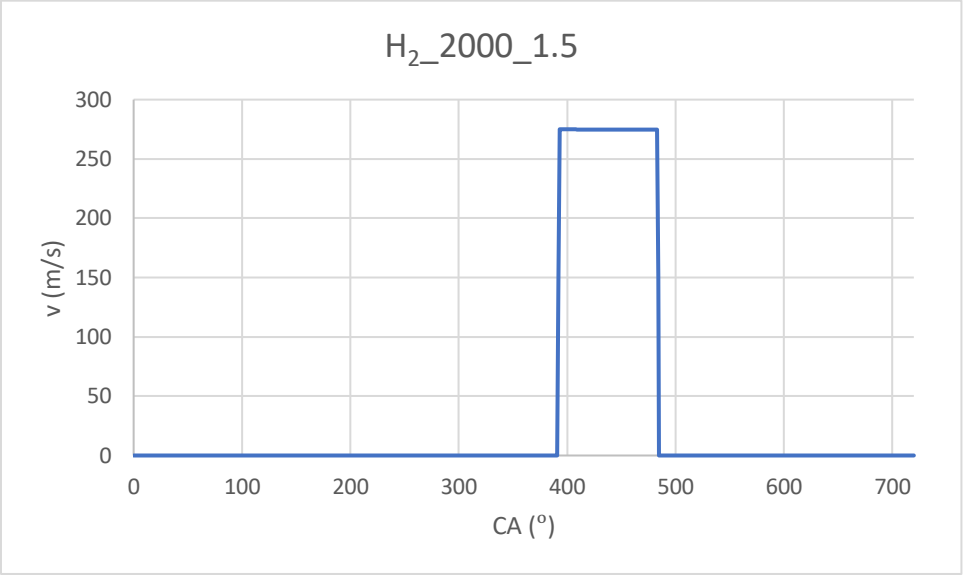

Figure C.1. Pulse Width (PW) profile of Hydrogen injection at 2000 rpm and lambda ratio of 1.5.

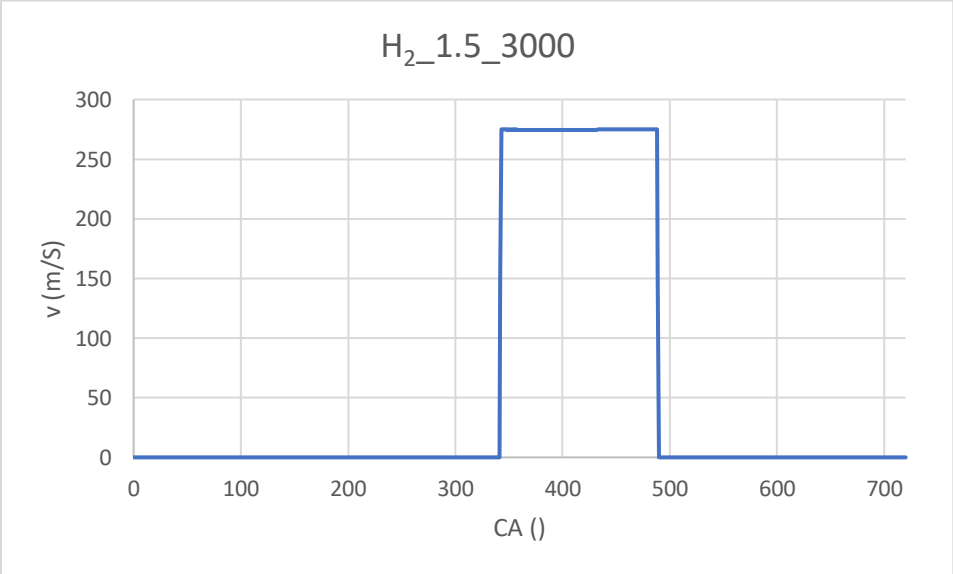

Figure C.2. Pulse Width (PW) profile of Hydrogen injection at 3000 rpm and lambda ratio of 1.5.

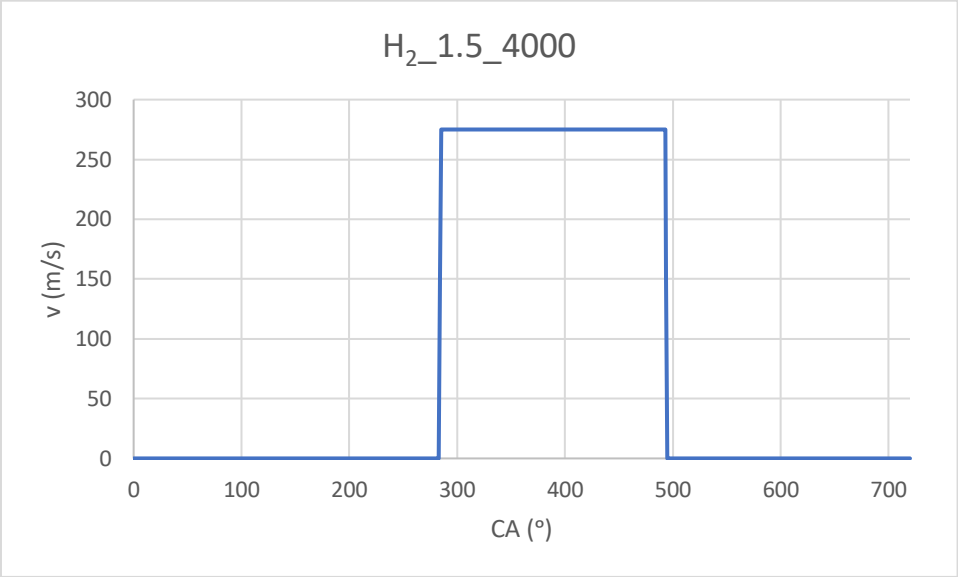

Figure C.3. Pulse Width (PW) profile of Hydrogen injection at 4000 rpm and lambda ratio of 1.5.

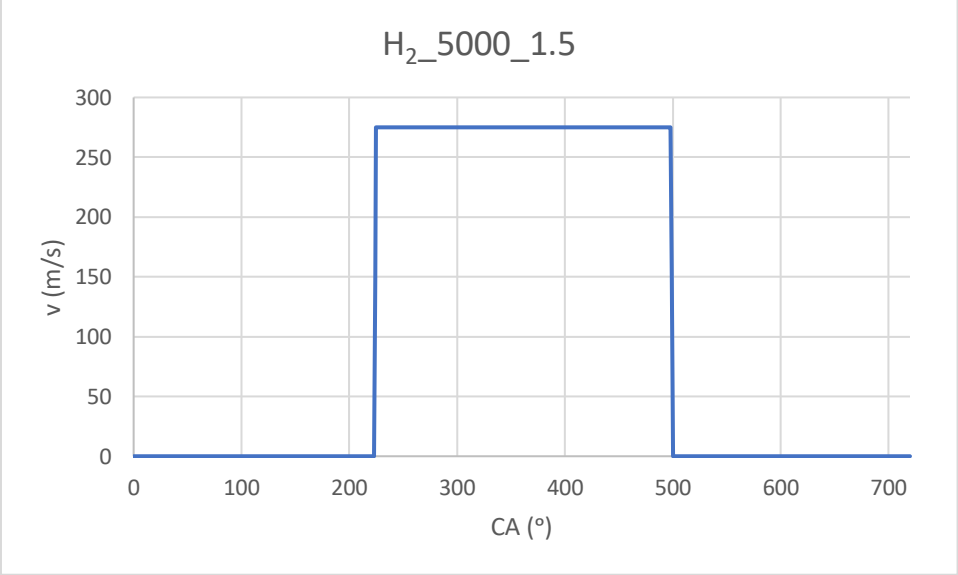

Figure C.4. Pulse Width (PW) profile of Hydrogen injection at 5000 rpm and lambda ratio of 1.5.

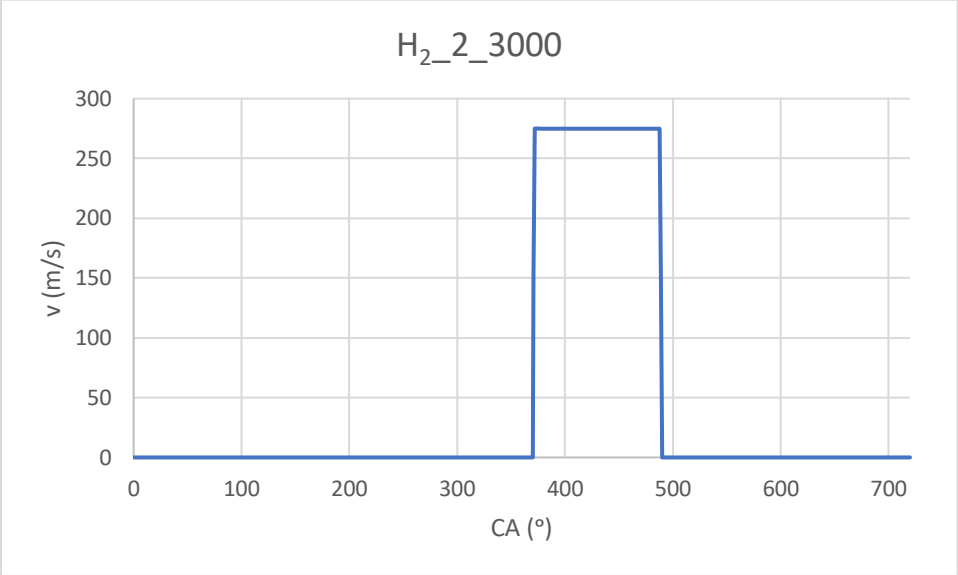

Figure C.5. Pulse Width (PW) profile of Hydrogen injection at 3000 rpm and lambda ratio of 2.

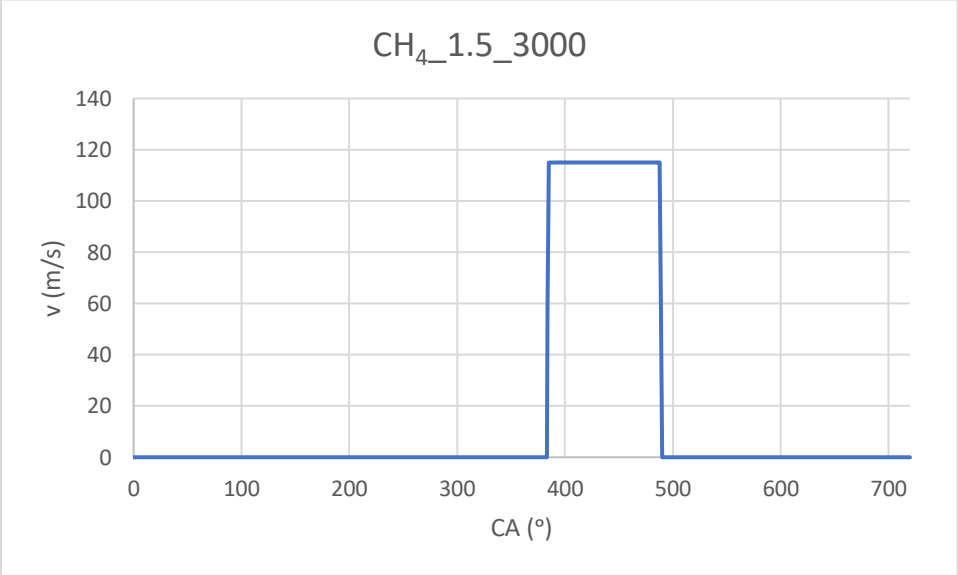

Figure C.6. Pulse Width (PW) profile of Methane injection at 3000 rpm and lambda ratio of 1.5.

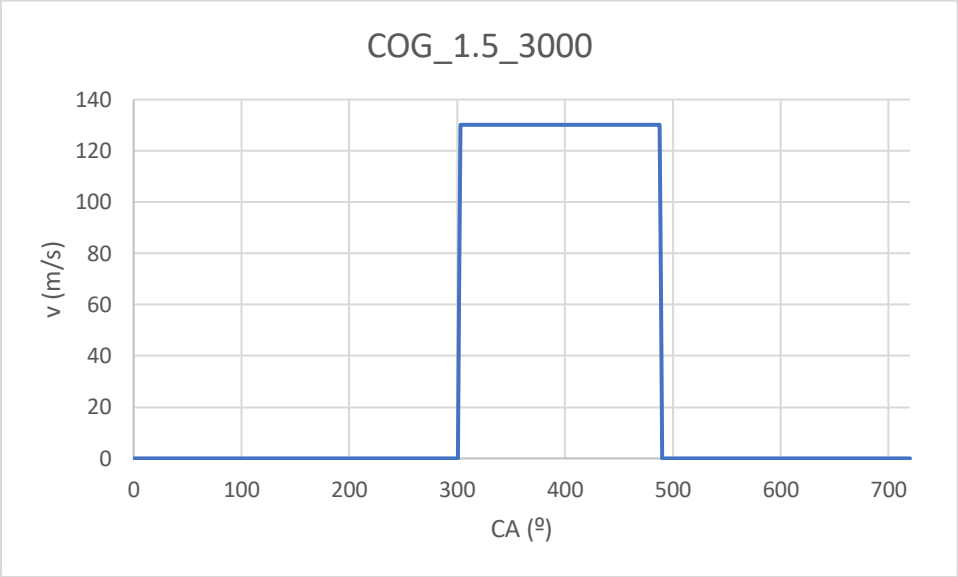

Figure C.7. Pulse Width (PW) profile of Coke Oven Gas injection at 3000 rpm and lambda ratio of 1.5.

Annex C. II. InValve and OutValve Lift Profiles.

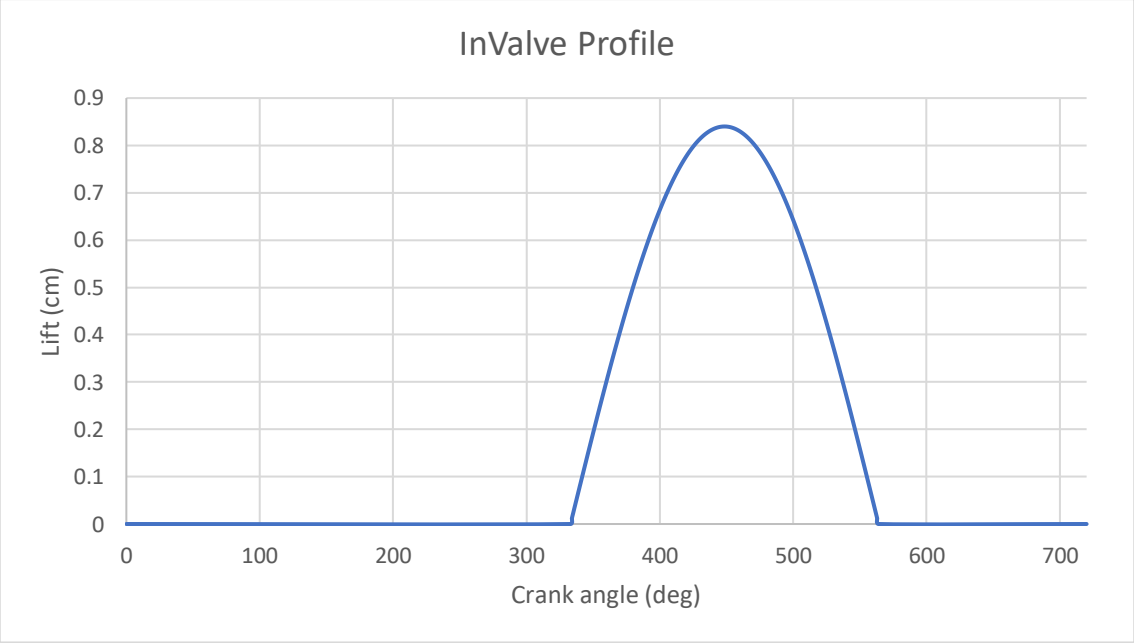

Figure C.8. InValve Lift Profile.

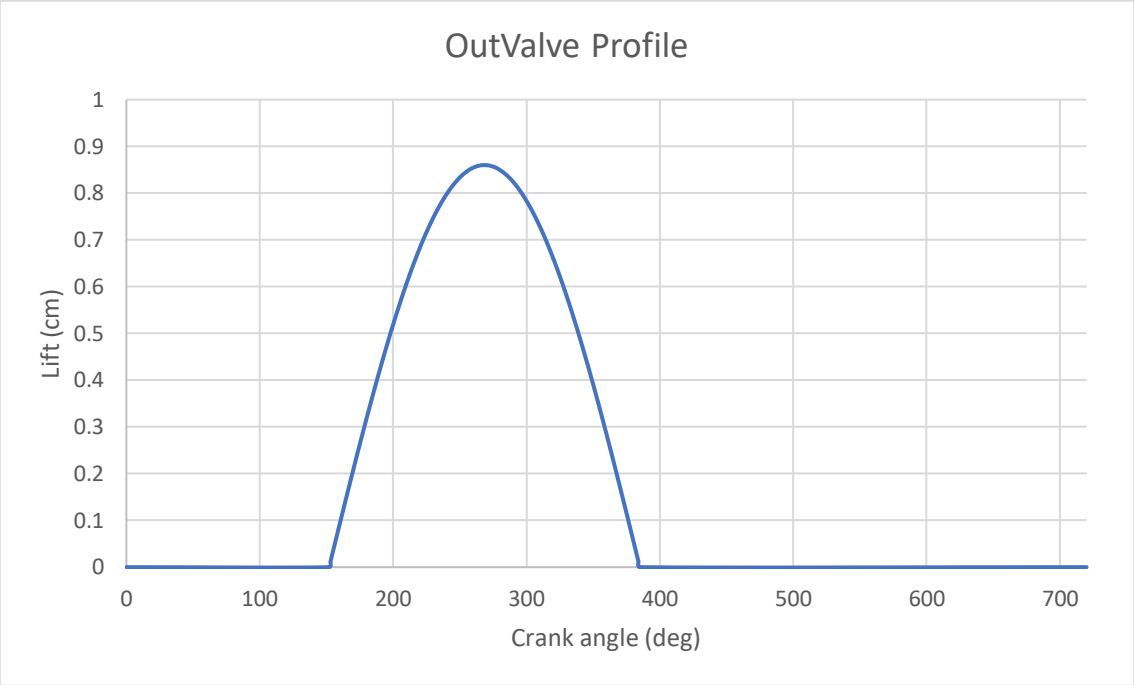

Figure C.9. OutValve Lift Profile.

Annex C. III. Tridimensional Pressure and Temperature graphs.

Injection.

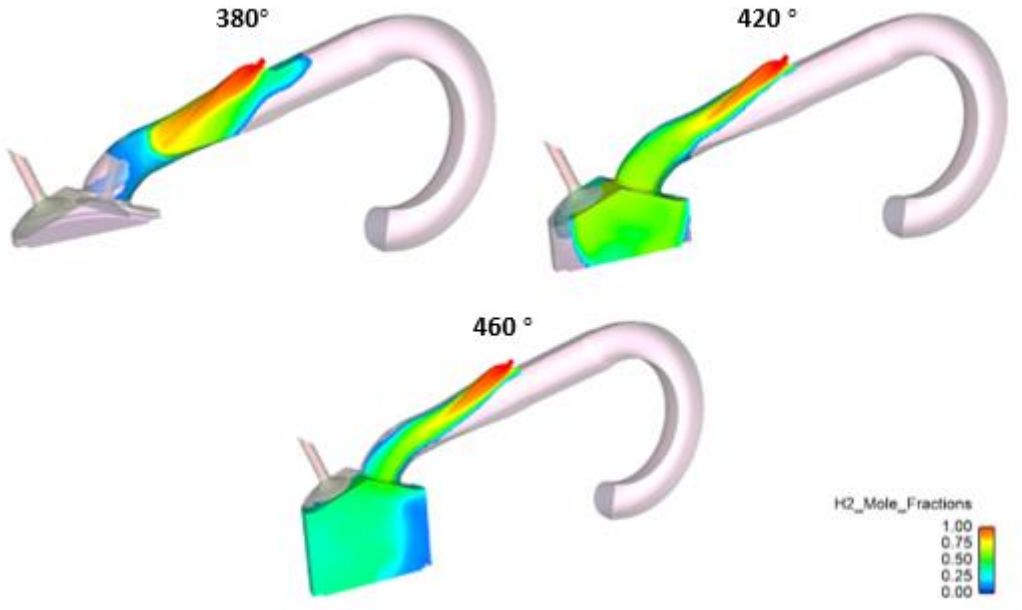

Figure C.10. 3D representation of the fuel injection during the admission stroke inside the cylinder and the intake manifold using H_2.

Temperatures.

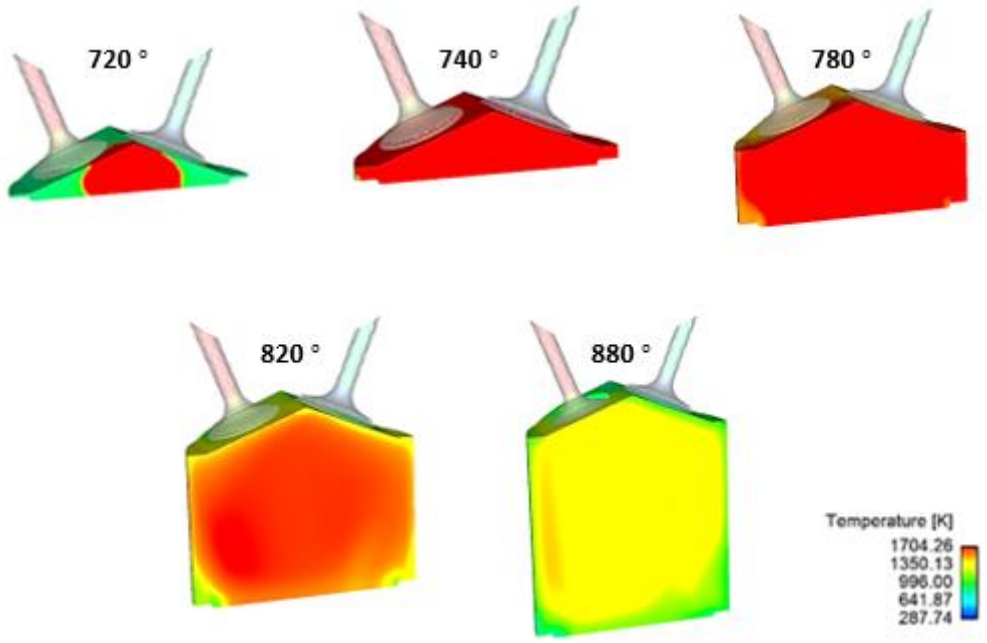

Figure C.12. 3D representation of the temperature changes during the combustion and expansion stroke inside the cylinder using H_2 at 3000 rpm and λ=1.5.

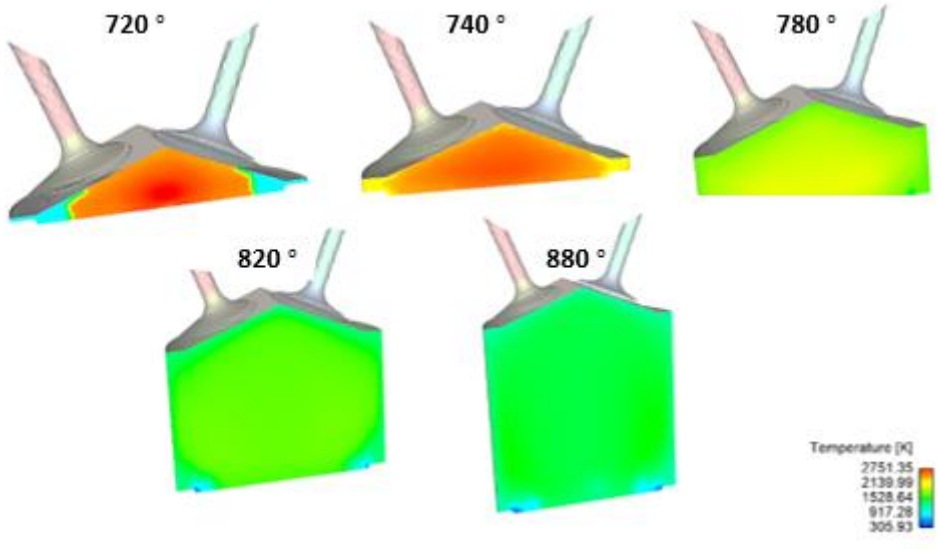

Figure C.11. 3D representation of the temperature changes during the combustion and expansion stroke inside the cylinder using H_2 at 5000 rpm and λ=1.5.

Pressures.

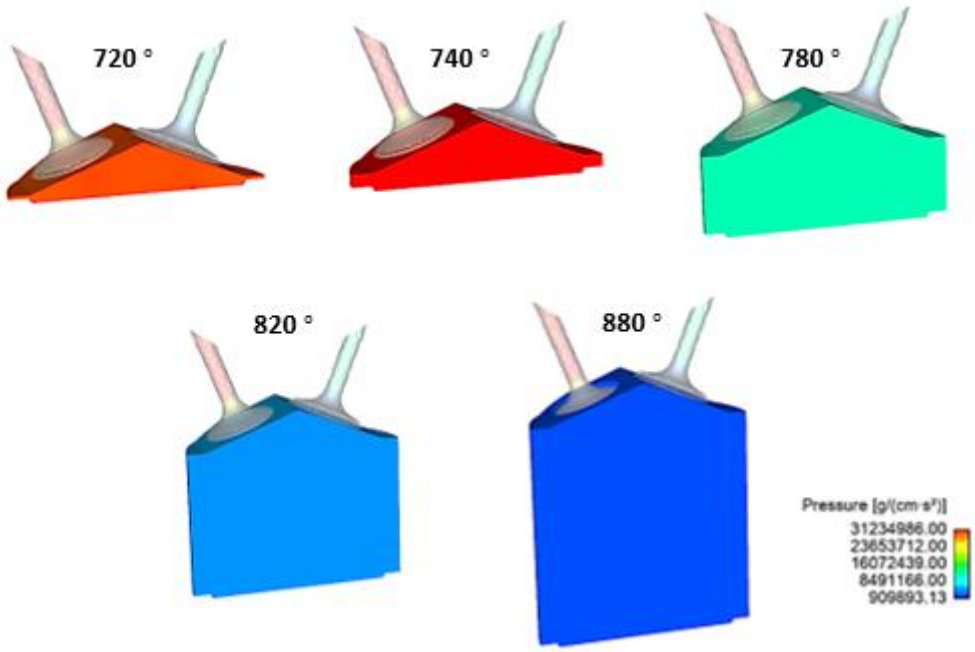

Figure C.13. 3D representation of the pressure changes during the combustion and expansion stroke inside the cylinder using H_2 at 3000 rpm and λ=1.5.

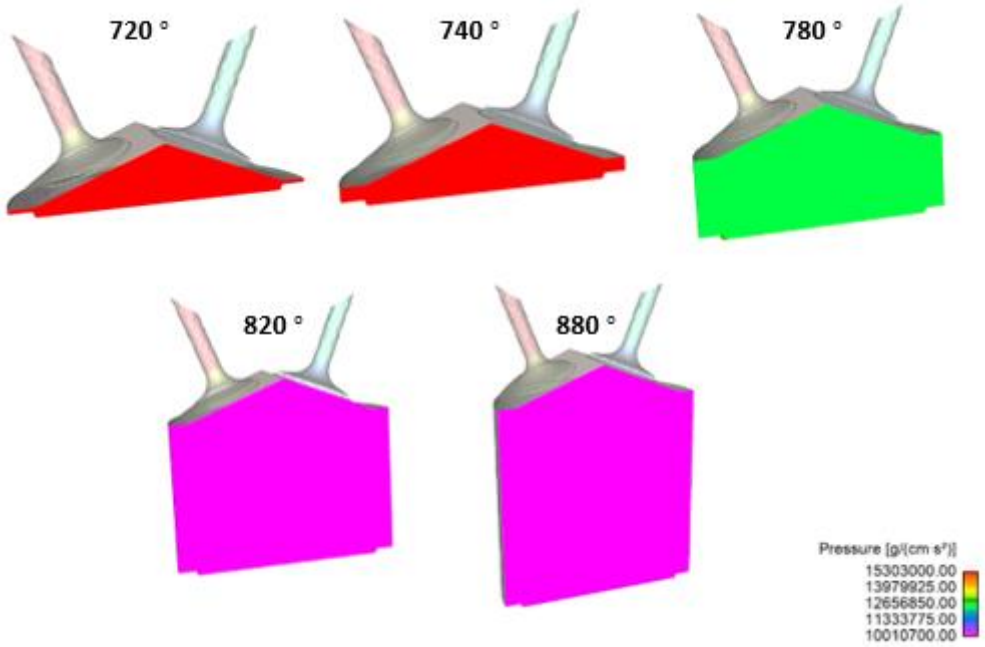

Figure C.14. 3D representation of the pressure changes during the combustion and expansion stroke inside the cylinder using H_2 at 5000 rpm and λ=1.5.

NO Mole Fraction.

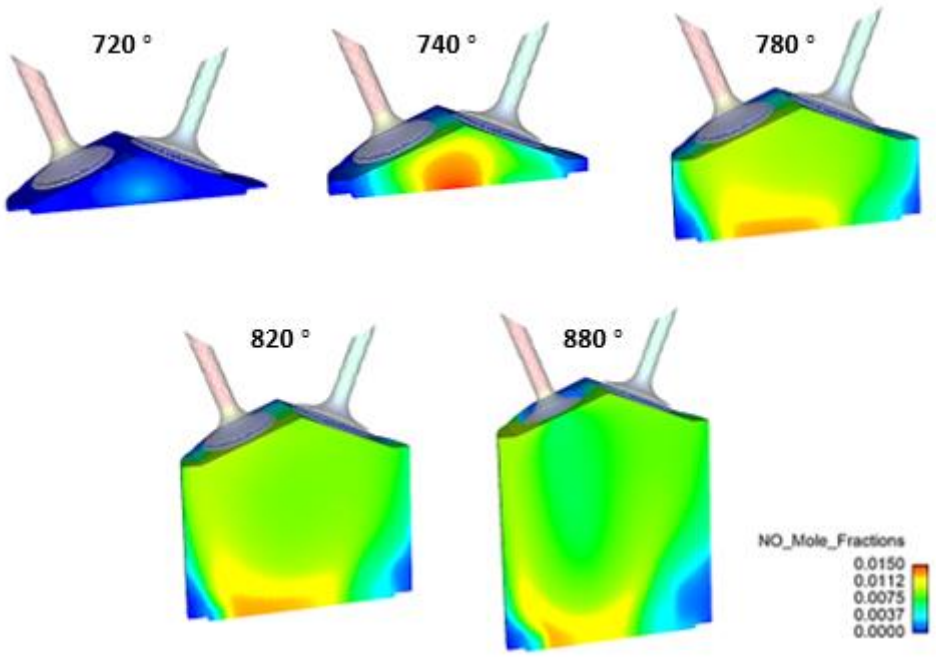

Figure C.15. 3D representation of the NO mole fraction changes during the combustion and expansion stroke inside the cylinder using H_2 at 3000 rpm and λ=1.5.

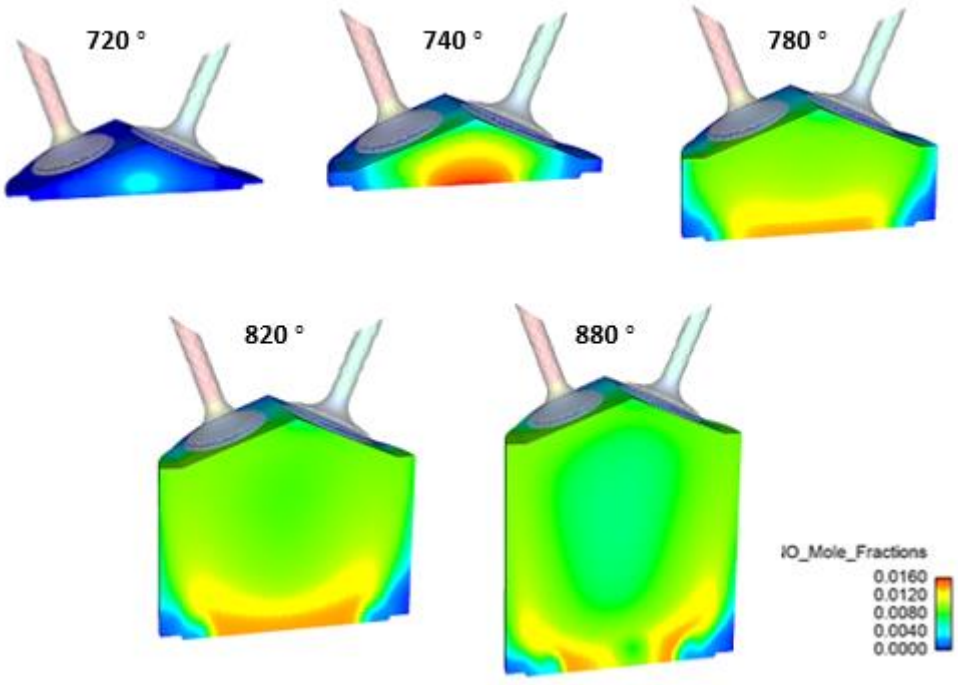

Figure C.16. 3D representation of the NO mole fraction changes during the combustion and expansion stroke inside the cylinder using H_2 at 5000 rpm and λ=1.5.